

NAVAL POSTGRADUATE SCHOOL
Monterey, California

①

AD-A280 778



DTIC
ELECTE
S F D
JUN 3 0 1994

DTIC QUALITY INSPECTED 2

THESIS

Space Experiments Aboard Rockets:
SPEAR III

by

James H. Morris

March 1994

Thesis Advisor:

R. C. Olsen

Approved for public release; distribution is unlimited.

94-19972



94 6 29 010

REPORT DOCUMENTATION PAGE			Form Approved OMB No. 0704-0188	
Public reporting burden for this collection of information is estimated to average 1 hour per response, including the time for reviewing instruction, searching existing data sources, gathering and maintaining the data needed, and completing and reviewing the collection of information. Send comments regarding this burden estimate or any other aspect of this collection of information, including suggestions for reducing this burden, to Washington headquarters Services, Directorate for Information Operations and Reports, 1215 Jefferson Davis Highway, Suite 1204, Arlington, VA 22202-4302, and to the Office of Management and Budget, Paperwork Reduction Project (0704-0188), Washington DC 20503.				
1. AGENCY USE ONLY (Leave blank)		2. REPORT DATE March 1994		3. REPORT TYPE AND DATES COVERED Master's Thesis
4. TITLE AND SUBTITLE SPACE EXPERIMENTS ABOARD ROCKETS: SPEAR III			5. FUNDING NUMBERS	
6. AUTHOR(S) James H. Morris				
7. PERFORMING ORGANIZATION NAME(S) AND ADDRESS(ES) Naval Postgraduate School Monterey CA 93943-5000			8. PERFORMING ORGANIZATION REPORT NUMBER:	
9. SPONSORING/MONITORING AGENCY NAME(S) AND ADDRESS(ES)			10. SPONSORING / MONITORING AGENCY REPORT NUMBER:	
11. SUPPLEMENTARY NOTES The views expressed in this thesis are those of the author and do not reflect the official policy or position of the Department of Defense or the U.S. Government.				
12a. DISTRIBUTION/AVAILABILITY STATEMENT Approved for public release; distribution is unlimited.			12b. DISTRIBUTION CODE	
13. ABSTRACT (maximum 200 words) The SPEAR III experiment was conducted in an effort to better understand and compensate for the effects of satellite charging, at levels up to KV. This experiment was designed as a lower-ionosphere test to both record vehicle charging and the effect of neutral-gas grounding systems. Prelaunch tests were conducted at the NASA-Plum Brook facility; launch took place at the NASA-Wallops facility. Electrostatic analyzer data provided a record of the rocket body potential, and indications of ion production, or energy-angle scattering within the plasma sheath. Plasma wave information was extracted from floating probe data and skin current probe data. Both provided sampling to resolve signals up to 10 KHz; the skin current probe also provided burst-mode sampling up to 500 MHz. There were no obvious signals in the 0-10 KHz data, other than a diffuse, low-frequency noise. The burst-mode data, acquired at the initiation of each 5-second charging sequence, showed a strong signal at around 100 KHz. This roughly corresponds to the lower-hybrid resonance frequency. It is possible, that LHR waves are responsible for energy-angle scattering of the ion flux accelerated to the charged rocket body.				
14. SUBJECT TERMS SPEAR III			15. NUMBER OF PAGES: 92	
			16. PRICE CODE	
17. SECURITY CLASSIFICATION OF REPORT Unclassified	18. SECURITY CLASSIFICATION OF THIS PAGE Unclassified	19. SECURITY CLASSIFICATION OF ABSTRACT Unclassified	20. LIMITATION OF ABSTRACT UL	

Approved for public release; distribution is unlimited.

**Space Experiments Aboard Rockets:
SPEAR III**

by

**James H. Morris
Lieutenant, United States Navy
B.S. University of Maryland, 1986**

**Submitted in partial fulfillment
of the requirements for the degree of**

**MASTER OF SCIENCE IN APPLIED PHYSICS
(SPACE SYSTEM ENGINEERING)**

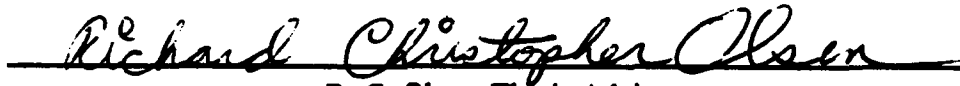
from the

**NAVAL POSTGRADUATE SCHOOL
Monterey, California
March 1994**

Author:


James H. Morris

Approved by:


R. C. Olsen, Thesis Advisor


S. Gnanalingam, Second Reader


William Bonisace Colson, Chairman
Department of Physics

ABSTRACT

The SPEAR III experiment was conducted in an effort to better understand and compensate for the effects of satellite charging, at levels up to 2 KV. This experiment was designed as a lower-ionosphere test to both record vehicle charging and the effect of neutral-gas grounding systems. Prelaunch tests were conducted at the NASA-Plum Brook facility; launch took place at the NASA-Wallops facility. Electrostatic analyzer data provided a record of the rocket body potential, and indications of ion production, or energy-angle scattering within the plasma sheath. Plasma wave information was extracted from floating probe data and skin current probe data. Both provided sampling to resolve signals up to 10 KHz; the skin current probe also provided burst-mode sampling up to 500 MHz. There were no obvious signals in the 0-10 KHz data, other than a diffuse, low-frequency noise. The burst-mode data, acquired at the initiation of each 5-second charging sequence, showed a strong signal at around 100 KHz. This roughly corresponds to the lower-hybrid resonance frequency. It is possible, that LHR waves are responsible for energy-angle scattering of the ion flux accelerated to the charged rocket body.

Accession For	
NTIS CRA&I	<input checked="" type="checkbox"/>
DTIC TAB	<input type="checkbox"/>
Unannounced	<input type="checkbox"/>
Justification	
By	
Distribution /	
Availability Codes	
Dist	Avail and / or Special
A-1	

TABLE OF CONTENTS

INTRODUCTION	1
I. HISTORY	2
A. INTRODUCTION	2
B. CHARGE II	4
C. THE SPEAR PROGRAM	7
D. SPEAR SERIES EXPERIMENTS	7
1. SPEAR I	7
2. SPEAR II	9
3. SPEAR III	9
II. SPEAR III	11
A. SPACECRAFT BODY	12
1. Sphere Bias System	13
2. High-voltage (HV) System	14
B. GROUNDING DEVICES	14
1. Hollow Cathode Plasma Contactor	14
2. Gas Release System	14
3. Thermionic Emitter	15

4.	Field Effect Device	15
C.	INSTRUMENTATION	16
1.	Charged Particle Detector	16
2.	Langmuir Probe	16
3.	Floating Probe	16
4.	Skin Current Probes	17
5.	High-Speed Data System	17
III.	SPEAR III PRELAUNCH TESTING	18
A.	INTRODUCTION	18
B.	THE PLUM BROOK TESTING CHAMBER	18
C.	RESULTS OF THE TESTING.	19
1.	Vacuum Results.	20
2.	Plasma Results.	20
IV.	FLIGHT OPERATIONS.	21
V.	OBSERVATIONS	23
VI.	DATA ANALYSIS	29
VII.	CONCLUSION	35

APPENDIX A: COLLECTED ILLUSTRATIONS	36
LIST OF REFERENCES	75
INITIAL DISTRIBUTION LIST	77

LIST OF TABLES

Table 1. SPEAR III Launch Time-line..	22
Table 2. Grounding Events.	24
Table 3. Flux Ratio Table	25
Table 4. Standard Constants.	29
Table 5. Gyro Frequencies.	30
Table 6. Plasma Frequencies.	31
Table 7. Lower Hybrid Frequencies	32

LIST OF ILLUSTRATIONS

Figure 1. Charge II.	36
Figure 2. Charge II I-V Curve.	37
Figure 3. Charge II Sheath Position.	38
Figure 4. SPEAR I Rocket Configuration	39
Figure 5. Magnetic Field Orientation.	40
Figure 6. SPEAR I Current Potentials.	41
Figure 7. SPEAR I ESA.	42
Figure 8. SPEAR III Configuration.	43
Figure 9. Sensor and Emitter Longitudinal Locations.	44
Figure 10. Neutral Pressure Gauge Position.	45
Figure 11. Sensor and Emitter Orientations.	46
Figure 12. Schematic of HV Capacitor Discharge Modes/Quiescent Mode.	47
Figure 13. SPEAR III Timing of High-speed Data System.	48
Figure 14. Simplified High-speed Data Schematic.	49
Figure 15. Plum Brook Plasma Chamber.	50
Figure 16. Mockup Physical Configuration.	51
Figure 17. Plum Brook Chamber Suspension.	52
Figure 18. Floating Probe Waveform - Shot 322.	53
Figure 19. Floating Probe Waveform - Shot 324.	54

Figure 20. SPEAR III Original Timeline.	. 55
Figure 21. Wallop's Digisonde.	. 56
Figure 22. SPEAR III Electron Density.	. 57
Figure 23. SPEAR III SAIC - 100 Seconds.	. 58
Figure 24. SPEAR III SAIC - 120 Seconds.	. 59
Figure 25. SPEAR III SAIC - 140 Seconds.	. 60
Figure 26. SPEAR III SAIC - 160 Seconds.	. 61
Figure 27. SPEAR III SAIC 170.770.	. 62
Figure 28. SPEAR III SAIC 170.962.	. 63
Figure 29. SPEAR III SAIC 170.994.	. 64
Figure 30. SPEAR III SAIC 171.634.	. 65
Figure 31. SPEAR III SAIC 171.666.	. 66
Figure 32. SPEAR III Floating Probe Spectrogram.	. 67
Figure 33. SPEAR III Floating Probe Line Plot.	. 68
Figure 34. SPEAR III Floating Probe Spectrogram of Entire Flight.	. 69
Figure 35. SPEAR III Skin Current Spectrogram.	. 70
Figure 36. SPEAR III Skin Current Probe @ 134.714.	. 71
Figure 37. SPEAR III Skin Current Probe @ 137.226.	. 72
Figure 38. SPEAR III Skin Current Probe @ 196.753.	. 73
Figure 39. SPEAR III Skin Current Probe Spectrogram of Entire Flight.	. 74

LIST OF EQUATIONS

(1) Charge Decay Calculation	13
(2) Non-charged Flux	25
(3) Charged Peak Flux	25
(5) Calculation for Plasma Frequencies.	30
(6) Lower Hybrid Frequency.	30
(7) Geometric Mean Gyrofrequency.	31
(8) Ion Sound Velocity.	32
(9) Electrostatic Ion Wave	32

ACKNOWLEDGEMENTS

I would like to express my appreciation to Professor Chris Olsen for his guidance and expertise in the data analysis and graphical computer programming. Without such assistance the writing of this paper would not have been possible. I would also like to express appreciation to John Antoniadis, Paul Rodriguez, Carl Seifring, and Dave Walker, scientists at the Naval Research Laboratory, Space Plasma Division. Their assistance in the SPEAR III Plum Brook data analysis during my six-week experience tour gave me the foundation to analyze the flight data.

I would also like to thank Douglas Potter at the Science Applications International Corporation (SAIC). His assistance in interpreting the electrostatic analyzer data and permission to use the data were paramount in the findings of this paper.

INTRODUCTION

Space electronic systems operate in a plasma environment which can adversely affect their operation. Degradation of command and control systems is more noticeable when operating high-power and high-voltage systems compared to lower electrical activity systems. The phenomenon that occurs is termed "spacecraft charging," which degrades the lifetime of satellites and systems integrity. Arcing, due to the accumulation of charges, is one of the main causes of phantom commands. Space defense systems require higher powered systems, which in turn increases the level of spacecraft-to-environment interaction. The power levels for space-based defense systems is estimated to be 100 kilowatts to 10 megawatts, and this level may require generation at some high repetition rate. Accomplishing the goal of effectively grounding a spacecraft requires an understanding of the space environment and the development of some effectual grounding scheme.

The effect of high-power discharge in the upper ionosphere is still not well understood. The environment in which this experiment is designed to occur is the ionosphere below 300 kilometers. This portion of the atmosphere is a weakly ionized plasma. As such, this environment offers the advantage of producing effects in "macro proportion" to those that might be seen in true space. In this respect, measurements are comparatively easy to obtain and analysis in a straightforward exercise.

I. HISTORY

A. INTRODUCTION

Dwight Duston, the Strategic Defense Initiative Organization (SDIO) Innovative Science and Technology director, has worked to keep the United States space experimentation programs moving forward. He has been one of the key leaders in the development of space systems such as Thunderbolt and the space-based rail-gun systems. He has stated "We're the only organization in DOD has specified space as our battleground. In general, the weapons systems environment is not a big deal but it is for us because we have got to deal with space. The limitations and potential leverage of environmental factors must be clearly understood to increase existing systems capabilities and performance and to optimize the design of new systems [Ref. 1]." Dwight's outlook was responsible for weapons systems environmental research, such as Queen Match, the Janus experiment, Red Gemini, the Sounding Rocket Measurements Program, and many others. Information from these experiments has been collected to build a strong knowledge-base for further study of the ionosphere [Ref. 2].

With the advancement of Strategic Defense Initiative (SDI), now known as Theater Ballistic Defense (TBD), the changing phenomenology of the space environment has become an area of major interest and study. Even with the realignment of SDI, ionosphere research for future strategic systems continue. There are many reasons for this interest. First, not only

does the problem of spacecraft charging impede the progress of development of space-based weapons systems, but it will eventually begin to stunt research into forms of high-energy propulsion and space-station design. Secondly, information about spacecraft charging will become increasingly important to space-support industries that wish to enter into space-based activities such as manufacturing of critical civilian and military components.

In the 1980's several programs were initiated to build a catalogue of information relating space-based weapons and the space environment. Some of the programs that have contributed to a better understanding of this environment are:

- ***Infrared Background Signature Survey (IBSS)*** — One of the most complex shuttle missions that provided information on the space background and plumes. These experiments utilized a cryogenically cooled infrared radiometer and spectrometer along with ultraviolet and visible spectragraphs and images to study chemical and rocket plumes [Ref. 3].
- ***Cryogenic Infrared Radiance Instrumentation for Shuttle (CIRRIS)*** — This set of experiments studied the energetic particles around the aurora of the Northern and Southern Lights. This is of interest because the spatial structured emissions during an aurora may emulate reentry vehicles [Ref. 4].
- ***Charge II Experiments*** — Studied the spacecraft charging and sheath formation in the ionosphere. Designed to investigate the electrodynamic interactions of a tethered system with the ambient ionosphere plasma and phenomena associated with the injection of electron beams from spacecraft [Ref. 5].

- ***The Defense Nuclear Agency (DNA)*** — Is also funding research into high-voltage power sources and power conditioning elements for space utilization. Their interest has been the development of high-voltages from 50 kilovolts to several megavolts with high repetition rates for generation. It is this DNA requirement that led to feasibility studies of high-voltage systems in space [Ref. 6].

The DNA has additionally funded experiments that investigated the phenomenon of spacecraft charging due to high-voltage (HV) discharges in low earth orbit (LEO). Space Experiment Aboard Rockets (SPEAR) was conceived to explore the feasibility of operating HV power systems in LEO. DNA funded SPEAR I, II, III, and vacuum chamber tests conducted at the NASA-Lewis Plum Brook Station [Ref. 7].

B. CHARGE II

A forerunner of SPEAR series that deserves further mention is the Charge II experiment. The Charge II payload was launched on a Black Brant IX from White Sands Missile Range in New Mexico in December 1985. The Charge II consisted of two sections called Mother and Daughter. The prime purpose of the flight was to study the interactions of the tethered system within the ambient plasma, and study the effects of electron beam emissions from the spacecraft.

The spacecraft consisted of two sections as shown in Figure 1. The Mother section consisted of the electron beam accelerator, floating probe array, current monitor for the

tether, high voltage supply and electron beam photometers. The floating probe consisted of four, gold-plated spheres mounted on a plastic telescope boom at radial distances of 25, 50, and 100 centimeters from the rocket skin. The floating probe array (PLP) was used as a floating probe to estimate the Mother potential and as a Langmuir probe to measure the electron density. The Daughter section consisted of the communication equipment and the charge probe. The purpose of the Daughter was to provide a reference plasma potential outside the disturbed regions generated due to the experiments on the Mother. The Mother and Daughter were connected electrically through an insulated tether.

The plasma current and potentials were measured throughout the experiments and then compared to models. One model in particular that appeared to have been successful in describing the structure of the potential sheath is the NASCAP/LEO model. The code for this model was created to calculate current collection, surface charging, and plasma sheath potential for the Charge II experiment. The model allows for the non-symmetric shape of the spacecraft. In the code the model is considered a 12 sided cylinder with a nose cone. The area of the model was 4.63 meters square verse the 4.68 square meters of the original. The surfaces of the model were considered to be perfect conductors for the purpose of ion collection. The grid used in the model would have a resolution of 21.5 cm. and 10.8 cm. close to the rocket. In the area of the PLP the resolution is about 2.7 cm.

The payload characteristic I-V plot is shown in Figure 2. The squares are the data points for the period when the spacecraft was on the up-leg to apogee. White circles are the down leg of apogee and black circles are the model predictions. The currents in the plot are normalized with the ion thermal current to the Mother when stationary in a plasma rest frame.

The calculations for this plot included computation with a plasma density of $4 \times 10^5 \text{ cm}^{-3}$. Simulations were completed with and without the effects of the magnetic field. It was observed that the field had a very small effect on what is observed both in the model and from the data observation. A possible reason was that the Larmor radius was large compared to the size of the payload and was large compared to the plasma sheath generated by the Mother section. Figure 3 shows the sheath position from the Mother payload skin estimated from the flight experiments and that predicted by the model. In this plot we see that the model is in agreement with the observation. We also note that the sheath is not of a constant size but varies with the potential.

Though the model was good at predicting most observations, it still deviated by approximately 15% to 20% as shown in Figure 2. With an increase in the negative bias potentials, the observed current increased more rapidly than the model predicted. A possible explanation for this is scattering by some mechanism or electron emission from the payload skin as ions bombard the spacecraft surface [Ref. 8].

We may conclude from the Charge II experiment that the following are true:

- ▶ The magnetic field had little effect on the flow of current .
- ▶ The velocity of the rocket gave an increase of about twenty percent to the ion current, relative to the Mother payload.
- ▶ The dimensions of the potential sheath do fluctuate with the applied potential to the payload.
- ▶ Secondary electrons are emitted from the spacecraft body, or there exists some other mechanism of electron generation.

C. THE SPEAR PROGRAM

The DNA funded a series of experiments that would investigate the effect of a highly charged, HV system in the space environment. The SPEAR series of experiments, started in 1987, had the primary goal of examining the feasibility of high-power operations in space. The SPEAR I experiment rode on a sixty-foot Black Brant IX sounding rocket, and the SPEAR II and III experiments rode on a sixty-foot Black Brant X sounding rocket. All experiments were launched from the Wallops Island NASA facility. Prior to each launch, the payloads were tested in the NASA-Lewis B2 vacuum chamber.

D. SPEAR SERIES EXPERIMENTS

1. SPEAR I

SPEAR I was launched December 13, 1987. SPEAR I was the first in a series of experiments to test the physics of developing and designing HV systems for space applications. The payload consisted of two, 20 cm. diameter spheres separated by a distance of thirty-nine inches (see Figure 4). The spheres were constructed from aluminum and plated with gold over nickel. The spheres were separated by a gradient ring section of eighty-two inches to ensure a uniform potential drop from the main portion of the boom to the two spheres.

The main body consisted of six sectors, each performing independent functions. The first section contained the photometers, Low-Light T.V. (LLTV), and the neutral pressure gauge. The second section contained the high-voltage power supply and capacitor circuits. This section generates the bias voltage applied to the spheres. Section three contained the measuring devices, Langmuir probe, wave receivers and the particle detector. After the measuring devices there are the attitude control system and finally the plasma contactor.

The attitude control system's primary purpose is to align the spacecraft with the magnetic field as shown in Figure 5. Changing the spacecraft alignment allows for the collection of data and analysis of interactions between the geomagnetic field and the high-voltage system. The V-plane of the booms was oriented to be near perpendicular to the magnetic field during the first portion of the flight. The attitude control system positioned the spacecraft so that the V-plane of the booms was parallel to the magnetic field. The last orientation maneuver placed one sphere-boom parallel to the geomagnetic field.

Two vacuum chamber tests were conducted as a mock up test before launch. The chamber tests were conducted at the University of Maryland plasma chamber facility and the second test was conducted at the NASA-Lewis Plum Brook B-2 chamber. The mock-up tested the circuit, equipment robustness and survivability to arcing and high-voltages in a plasma environment. The integrity of the spacecraft high-voltage circuits and experiments were validated and proven to be sound [Ref. 9].

Observation of the chamber test showed a glow around the spheres suggesting plasma breakdown. It was generally believed that this breakdown would occur when more than a

few kilovolts were applied to exposed electrodes in a plasma chamber. The effect was also expected at altitudes above 100 km. The LLTV did not detect any arcing between the spheres during the entire flight. Figure 6 shows plots of current and potential versus mission time. The decay in these plots are typical of a capacitor discharging into a linear resistance. The exponential decay shown here implies that there was no plasma breakdown during the flight confirming the LLTV data. The spikes observed are considered to result from a damped oscillatory current and were found in all current data plots. The I-V plots at the bottom of Figure 6 show a linear relationship, indicating the system impedance was nearly constant. The plasma impedance was about $1\text{ M}\Omega$ [Ref. 10].

Electrostatic analyzer data from SPEAR I showed ions accelerated into the (negatively charged) rocket body. Van Horn, in his thesis on SPEAR I at the Naval Postgraduate School, analyzed the charging behavior of SPEAR I with such data. Note that in addition to the charging peak, there is a diffuse spectra below the peak. These were considered to be ions formed or scattered in the sheath (see Figure 7).

2. SPEAR II

SPEAR II was designed to test new high-voltage components and also carried the first rail-gun into space. After the launch, the rocket guidance system failed and the booster was destroyed thirty-five seconds into the launch. Even though the flight ended in disaster, information was gained about the design of HV circuits that would be utilized on later flights. The chamber experiments of the new HV designs would be employed in the next SPEAR experiment.

3. SPEAR III

SPEAR III, the most recent experiment in the sounding rocket series, was designed similar to SPEAR I. However, instead of using two spheres, only one was used as shown in Figure 8. This figure illustrates the Weitzmann Boom onto which the floating probe was attached and the sphere extended.

Some of the scientific objectives of SPEAR III were:

- (i) Test several grounding mechanisms when the body reached several negative kilovolts.
- (ii) Diagnose physical mechanisms of the grounding techniques.
- (iii) Study the dispersion of gaseous effluent emitted from a space platform.
- (iv) Test the effectiveness of the grounding techniques in reducing local differential charging on a diagnostic probe and on solar cells.
- (v) Monitor the undisturbed and disturbed plasma and neutral gas environments of the payload.

The sections which follow address the data obtained in this mission.

II. SPEAR III

SPEAR III, the most recent experiment in the sounding rocket series, was similar to SPEAR I in design. As in previous experiments, testing prior to launch was conducted at the NASA-Lewis B2 vacuum chamber. The SPEAR III rocket was launched March 15, 1993, at 21:13 EST. SPEAR III reached an apogee of 289 km., 278 seconds after launch from NASA-Wallops.

SPEAR III science objectives, per the previous section, largely arose from unanswered questions from SPEAR I, and new concerns about differential charging, and the control thereof. The primary purpose of this work is to further address the return ion fluxes observed on SPEAR I, and attempt to explain the (apparent) scattering process observed there.

To achieve the SPEAR III science objectives, new grounding schemes were designed to be implemented during the space flight along with circuitry similar to that of SPEAR I. These methods, discussed below, are:

- (i) Ambient Gas
- (ii) Thermionic emitter
- (iii) Field Effect Device
- (iv) Gas Release System
- (v) Hollow Cathode Plasma Contactor

Another objective of SPEAR III was to study the effect of slow versus fast HV charging, and again address questions as to the effect of orientation relative to the geomagnetic field.

A. SPACECRAFT BODY

The rocket used for the launch was a Black Brant X rocket. It is composed of three stages of solid fuel which are, Terrier Booster, Black Brant 5c, and Nikha. The diameter of the rocket was seventeen inches. The scientific equipment was housed in the rocket body as illustrated in Figure 9. The five modules that were important to the SPEAR III experiment were the nose cone, HV module, Science 1 package, Science 2 package, and the Science 3 package.

The nose cone consisted of the HV boom and sphere assembly, the aft viewing Low Light Level Television Camera (LLLTV), and forward viewing LLLTV camera. The HV Module was fifty-four inches long and contained primary battery power, the HV power supply, HV capacitors, switching network, current and voltage monitors, and the signal conditioning unit. Science 1 was thirty-eight inches long and contained the two energetic particle detectors, solar cell system, two skin current probes, differential charging device, electron emitter, field-effect device, magnetometer, and a three-channel fast data unit. Science 2's length was fifty-four inches and contained another fast data unit with three channels, the neutral pressure gauge system, transient pulse monitor, two additional skin current probes, differential charging device, gas release system, hollow cathode plasma

contactor, Langmuir probe electronics, and floating probe electronics. Science 3 was eighteen-and-a-half inches in length and contained the Langmuir probe and boom, and the floating probe and boom.

Figure 10 shows the location of the neutral pressure gauge, hollow cathode plasma contactor, Langmuir probe, and the neutral gas release system jets. Figure 11 details the sensor and emitter orientations viewed aft of the payload.

The two charging circuits shown in Figure 12 were designed to charge the sphere to the required potential. The two high-voltage circuit-charging devices, a switched fast and a ramped, were designed to charge the sphere to the same potential. A charging device was designed to charge the sphere for each grounding device. Each charging event was conducted over a five second interval [Ref. 11].

1. Sphere Bias System

The sphere was pulsed positive with respect to the payload. To complete the circuit the plasma in space provides the ions or electrons, depending on the sphere potential.

Charging the sphere positive forces the body negative. The expected charge decay is described for positive voltage as:

$$V_c = V_0 e^{-\frac{t}{RC}}$$

(1) Charge Decay Calculation

This type of charge decay was seen in the SPEAR I data, per Figure 6, from the SPEAR I flight. This similarity validates this conceptual approach to the SPEAR experiments. These

figures validate the SPEAR I chamber results as well as validating the accuracy of the SPEAR III data set. The type of decay seen in the Figure 6 indicates that for a properly designed system, the plasma would not break down for ionospheric systems [Ref. 12].

2. High-voltage (HV) System

The high-voltage system provided a differential bias between the deployed sphere and the vehicle to drive the vehicle to negative potentials. A twenty kilovolt power supply was used to charge a capacitor which is connected to the deployed sphere. Figure 12 is a drawing of the HV circuits. The incorporation of RC components is also shown in that illustration. Also shown are the differences between the ramped, fast and quiescent mode of the circuit design. It is these circuits that quickly charged the sphere, which in turn forced the body negative [Ref. 13].

B. GROUNDING DEVICES

1. Hollow Cathode Plasma Contactor

The plasma contactor is a hollow cathode gas discharge that is capable of generating a dense plasma. It generates 0-10 amps current at bias levels greater than -100 volts. The plasma contactor was designed to produce a high plasma density in the vicinity of the vehicle which results in an electrically low impedance path between the vehicle and the ionosphere [Ref. 14].

2. Gas Release System

The gas release system was designed to release non-corrosive gases through four nozzles. The flow rate was a max. of one gram/second to a lower limit of .02 grams/second. The torque induced upon the spacecraft was designed not to exceed 1/100th of the minimum torque generated by the ACS. The gas was discharged tangential to the cylindrical skin of the payload, and perpendicular to the longitudinal axis of the payload. This provided a high density neutral gas cloud in the vicinity of the vehicle so that additional plasma is generated by collisional ionization, thereby creating an electrically low impedance between the vehicle and the ionosphere. The plume formations were two opposed pairs, with each pair on opposite sides of the rocket body [Ref. 15].

3. Thermionic Emitter

The Thermionic emitter is basically a device similar to a heating element. The element was three percent rhenium-tungsten wire (0.008" diameter). The maximum operating temperature expected was 3073 degrees Kelvin. The design lifetime was ten hours.

A tungsten metal cathode protruded into the plasma sheath where when heated would emit electrons into the plasma sheath. Emissions were limited to a maximum of one ampere in current. The concept here is to utilize the negative charge of the spacecraft body for the transfer of electrons to the plasma. The intended result of this emitter is a rapid ground for the spacecraft [Ref. 16].

4. Field Effect Device

The Field Effect Device is an array of collected fine points. These fine points will be the focus of charge accumulation. This procedure utilizes negative charge of the

spacecraft body and the electric field to cause emissions through the sharp tips of the device. The net result here will be a reduction of the negative charge of the spacecraft after being discharged through a plasma [Ref. 17].

C. INSTRUMENTATION

1. Charged Particle Detector

The charged particle detector was developed by Science Applications International Corporation (SAIC). The analyzer utilizes curved plates biased to collect positive ions in a predefined energy bandwidth. Two pairs of sensors were used, with different geometric factors. The electrostatic analyzer (ESA) generates an energy spectrum of the ions in the plasma sheath. The geometric factor used here for the high sensitivity ESA is $3.4 \times 10^{-5} \text{ E} \cdot \text{sec} \cdot \text{cm}^2$ [Ref. 18]. The energy resolution is seven percent and the energy ranges are 12 to 897 electron volts and 0.39 to 29 kilo electron volts. The time resolution was 32 ms. per sweep, 1 ms. per sample [Ref. 19].

2. Langmuir Probe

The Langmuir probes were mounted flush with the vehicle skin. The probes measured the distribution of return currents to the vehicle at different locations with respect to the grounding systems. Figure 10 shows the location of the probe [Ref. 20].

3. Floating Probe

The floating probe was a spherical device deployed three meters from the spacecraft body on a boom. The purpose of the probe was to measure the potential difference

between the vehicle and the sphere when the spacecraft body is negative. It was expected that the probe would be beyond the plasma sheath when the vehicle was -300 volts. The floating probe also gave an indication of the effectiveness of each grounding mechanism. Figure 8 shows the position of the probe during deployment, and Figure 12 shows how it was connected to the HV circuit in the modes of operation [Ref. 21].

4. Skin Current Probes

The skin current probes were plane current collectors mounted flush with the vehicle skin. The range of the instrument was 500mA/m^2 to 50mA/m^2 . The probes were designed to measure the distribution of return currents to the vehicle at different locations near and remote to the vehicle [Ref. 22]. The output from the skin current probes provided one of the inputs for the high-speed data system.

5. High-Speed Data System

A high-speed digitizer was incorporated in the design to capture the data and store it into a cache memory. The sample interval was one microsecond. Low pass filters were used to prevent aliasing. Figure 13 is a simplified high-speed data schematic. A 300 KHz low-pass filter was used on the Rogowski current coil and the sphere voltage measurement. The skin current was filtered with a 150 KHz low-pass filter. In accordance with the Nyquist sampling theorem, the largest observable frequency is .5 MHz. Figure 14 is a diagram of the digitizer circuit and the sampling cycle [Ref. 23]. Note that data are acquired in a 16 ms. "snapshot" beginning just before the high-voltage is switched.

III. SPEAR III PRELAUNCH TESTING

A. INTRODUCTION

The NASA-Lewis Plum Brook Station vacuum chamber was used to test SPEAR III prior to launch.

B. THE PLUM BROOK TESTING CHAMBER

The NASA Plum Brook Station B-2 vacuum chamber is a large, cylindrical chamber configuration measuring approximately 13 meters in diameter and twenty meters high. The chamber is pumped by twelve, 90 cm. diffusion pumps to a minimum base pressure of 2.5×10^{-6} Torr. During the experiments, the high-voltage was applied to booms while the rocket body was held at ground potential.

This chamber has been used for testing of payloads for various rocket projects. This facility provides the capabilities of testing payloads in vacuum or in varying degrees of gas pressure and ion mixtures that may be set to parallel (or model) different conditions in the atmosphere. These conditions usually involve height and partial effects of vacuum on payloads.

Figure 15 shows the physical configuration of the spacecraft in the plasma testing chamber. The total length of the spacecraft body was 300 inches and an extender arm

exceeded this length by another eighty inches. The sphere was extended forty inches from the spacecraft body perpendicular to the extender arm. Two video cameras were mounted inside the chamber to observe the sphere. Their cables were fed through an insulated junction in the wall of the chamber. Fiber-optic cables were connected to the pulser, which were in turn connected to the relays and power controls, which also came through the insulated chamber bulkhead. Into the base of the spacecraft (see Figures 16 and 17) the fiber optic cable was connected as were the high-voltage ground cables. Support suspension for the mockup were connected to the base structure of the spacecraft and the boom. The suspension bolts did not have any effect upon the experiment.

C. RESULTS OF THE TESTING.

In the process of testing, the charging circuits were tested and skin potentials measured. Figures 18 and 19 are plots of the potentials during the vacuum test. The floating probe and the skin potential decay have approximately the same decay constant after charging. These results conformed to scientific expectations and validated the operation and design of the spacecraft and Weitzmann boom. The figures show the floating probe measurements with the vehicle skin potential. During the test there were no indications of plasma breakdown.

The results of the testing may be summarized in the following manner:

1. Vacuum Results.

- ▶ Boom orientation perpendicular to the magnetic field increases the breakdown threshold for the sphere above 10kV for pressures below 4×10^{-5} Torr. Oblique orientation in this chamber for the SPEAR I mockup was 4kV by comparison.
- ▶ Body sheath threshold was above 10kV.
- ▶ For pressures above 2×10^{-4} Torr the threshold drops below 5kV.
- ▶ The disrupter does not produce an observable change in the breakdown characteristics for voltages up to 10kV.

2. Plasma Results.

- ▶ For pressures in the 1×10^{-5} Torr range or higher, the sphere sheath broke down for voltages down to 200 V with plasma densities in the range of $1 \times 10^4 - 2 \times 10^5 \text{ cm}^{-3}$.
- ▶ The maximum voltage held by the negative body sheath was 1.5kV, possibly due to enhanced ion flux from the breakdown at the sphere.

These results were considered repeatable.

IV. FLIGHT OPERATIONS

SPEAR III was launched on a Black Brant 10 rocket. The booster was a Terrier MK70 motor, consisting of the MK12 motor case for better performance. The rocket booster had a case diameter of 18 inches and a length of 170 inches. The sustainer was the standard Bristol four-fin motor assembly. The dimensions of the sustainer were a case diameter of 17.26 inches and body length of 208 inches.

SPEAR III was launched from a rail launcher at 21:13 EST at the NASA-Wallops Flight Facility. Figure 20 illustrates the planned flight time-line. Figures 20 and 21 show the data from the Wallops Digisonde. The latter figure includes the density inferred from the Langmuir probe. Note that electron densities remain below $2 \times 10^5 \text{ cm}^{-3}$ throughout the mission. Figure 22 is a list of selected events pertaining to the writing of this paper.

The time line was executed as planned for the entire flight as well as activation of instruments and all attitude maneuvers. All three science attitudes were achieved with respect to the magnetic field. PCM data was collected for the entire flight and later processed by NASA at Wallops Island [Ref. 24].

Table 1. SPEAR III Launch Time-line.

<i>MET(s)</i>		<i>MET(s)</i>	
0.0	Launch	200	N. G.
69.0	payload separation	220	T. E.
71.0	eject nose cone	240	FED
71.4	instrument deployment	260	P. C.
76.0	science attitude 1	280	no ground
89.0	maneuver complete	281	science 2
91.0	deploy HV boom/FP	290	N. G.
95.0	charge HV capacitors	310	T. E.
95.1	turn on ESA HV	330	FED
100.0	first event/no ground	350	P. C.
110.0	neutral gas	370	no ground
130.0	T. E.	371	science 3
150.0	FED	400	N. G.
170.0	Plasma Contactor	420	FED
190.0	no ground	460	no ground
		470	N. G.

V. OBSERVATIONS

Observation and data analysis from wave and particle instruments were reduced and analyzed for this work. The particle data were examined to determine charging behavior and studied to see if substantial energy angle scattering was again occurring in the return ion flux. Figures 23 thru 26 show the initial 80 seconds of operation, and the majority of interesting features in the data. The data are shown as energy time spectragrams. The vehicle charged to slightly more than one kilovolt negative as the sphere bias is raised to ten kilovolts. The potential drops were exponential in time, with some exceptions. We also observed the exponential decay previously seen on SPEAR I (see Figure 6). Figure 23 at 110 seconds shows a dropout associated with a momentary discharge of the rocket body, probably due to a gas release. The lack of measurement or detection at 114 seconds is unexplained. The ESA data did not detect any difference between fast and slow ramp charging of the sphere.

In Figure 24 two sequences are shown which include operations of the thermionic emitter. The emitter is on for the shots at 130 and 135 seconds. Observe that at this low altitude (220 km.) the emitter worked extremely well in grounding the spacecraft. The ESA shows no ions above the 10 EV energy threshold. This appears to be due to the TED operation.

The grounding events that were in operation during the time-frame of the four SAIC spectragrams are:

Table 2. Grounding Events.

<i>MET</i>	<i>Event</i>
100-110	No Event
110-130	Neutral Gas
130-145	Thermionic Emitter Device (TED)
145-150	No Event
150-170	Field Effect Device
170-180	Hollow Cathode

It is the TED event at 130 seconds that completely grounds the spacecraft. For flux analysis, the Hollow Cathode is chosen at 170 seconds.

Data from the shot at 170 are shown in Figure 26. Line plots were made from this set of data (see Figures 27 thru 31) to analyze the phase space density and the distribution function. As seen in the figures, the low energy portion of the spectrum was least squares fitted (LSF), and from this we obtained the density and thermal temperatures. The charging peak was modeled (but not fitted) as a Maxwellian, accelerated through a potential drop. The parameters are also included in the figures. Table 3 summarizes what is found in the data. In the equations below, *flux* correlates to data not associated with the charging peak and *flux'* with that of the charging peak. In the table, "Low Peak" refers to that under the low energy and "Charging Peak" refers to what is observed under the charging peak. *kT* is energy that corresponds to flux as *kT'* corresponds to the potential peak. The "Ratio" is the ratio between *flux* and *flux'*. The equations for calculating the *flux* are:

$$flux_i := N_i \cdot \sqrt{\frac{kT_i q}{2\pi m}}$$

(2) Non-charged Flux

$$flux_i' := N_i' \cdot \sqrt{\frac{kT_i' q}{2\pi m}} \cdot \left(1 + \frac{\phi_i}{kT_i'}\right)$$

(3) Charged Peak Flux

The table representing the results of these calculations is as follows:

Table 3. Flux Ratio Table

Timing	Potential	Low Peak	Charging Peak	Ratio
171.634	480	$2.923 \times 10^{18} \cdot \text{m}^{-2} \cdot \text{sec}^{-1}$	$8.700 \times 10^{17} \cdot \text{m}^{-2} \cdot \text{sec}^{-1}$	3.241
170.77	1000	$4.270 \times 10^{18} \cdot \text{m}^{-2} \cdot \text{sec}^{-1}$	$5.499 \times 10^{17} \cdot \text{m}^{-2} \cdot \text{sec}^{-1}$	4.922
171.09	820	$4.144 \times 10^{18} \cdot \text{m}^{-2} \cdot \text{sec}^{-1}$	$9.174 \times 10^{17} \cdot \text{m}^{-2} \cdot \text{sec}^{-1}$	4.517
171.122	820	$4.515 \times 10^{18} \cdot \text{m}^{-2} \cdot \text{sec}^{-1}$	$9.174 \times 10^{17} \cdot \text{m}^{-2} \cdot \text{sec}^{-1}$	7.766
171.666	580	$2.820 \times 10^{18} \cdot \text{m}^{-2} \cdot \text{sec}^{-1}$	$8.700 \times 10^{17} \cdot \text{m}^{-2} \cdot \text{sec}^{-1}$	3.36

From the table we see that the low energy portion of the spectrum is larger than the flux in the charging peak by a factor of 3 to 8. This observed fact motivates a careful search for some process which can cause the unusual distribution of ions to be scattered with respect to energy and angle. The observation here is similar to what was found in the SPEAR I data.

The question which is motivated by the electrostatic analyzer data is, therefore: what is the source of the scattering which is apparently occurring here? The most likely place for finding an answer is in the electric field (wave) data, particularly from the floating probe and skin current probe. Data sampled at 20 KHz from both were studied, and the 1 MHz burst mode data were studied.

The floating probe should have detected any significant signals below 10 KHz. Figure 32 shows the fourier-transformed floating probe data for a 20 second interval. We see here constant line frequency signals throughout the time of the shot. The author classifies the frequencies here as mechanical artifacts. This floating probe plot was typical for the probe during the entire flight. The three orientations in the magnetic field did not have any apparent effect on any of the data analyzed. There was no noticeable effect in the floating probe data that would have been in the range of the cyclotron frequencies that are dependent on the magnetic field. The lack of any signal may imply that either the signals were masked by noise, or some other phenomenon was taking place that did not allow signal detection.

Figure 33 is a line plot of the electric field versus the frequency in KHz. The line plot here was typical of all the floating probe line plot data. The peaks that you see in the line plot at 2, 4, 6, and 8 KHz correspond to the frequencies in the spectrogram. The consistency of these signals throughout the entire flight supports our conclusion that they are mechanical artifacts of the spacecraft. Floating probe data for the entire mission are shown in Figure 34. This reinforces the lack of evidence for resonant signals which mirror physical processes. The low-frequency, diffuse spectra is apparent throughout the mission.

The skin-current probe plot Figure 35 shows the amplified vs. frequency and mission time. This spectrogram, a gray scale, shows that there are signals in the 100 KHz range. This is the burst mode data transformed into the frequency domain. Sixteen milliseconds of data were acquired at 1 MHz, shortly after the initiation of a sphere bias. These measurements are broken down into 32 segments of 0.5 ms. each, and transformed into the frequency domain. The resulting spectra are plotted as though they occurred over a 4.5 second interval beginning at the time the snapshot was acquired. The vertical black bands plotted are used to separate the snapshots. The 100 KHz signal shown in the plot appear to be characteristic of some real physical process. The intensity varies with grounding devices, but is always present.

Some of the strongest spectra were acquired at events from 130-145 seconds MET. Figure 35 is the ESA spectrogram of the time frame. Figure 36 and 37 are skin current line plots that correspond to the 120 time event. A broad peak is found around 100 kilohertz. This is a TED event where the ESA data showed no charge peak and where the potential of the rocket body remained below 10V in magnitude. It seems there is a profound relationship between current flowing in the spacecraft environment system and the oscillations observed here.

Somewhat more typical are data from 180 to 200 seconds Figure 38. Again we find broad peaks from wave data acquired at the start of each probe bias sequence. Also of interest is the lack of signal intensity during the ramp charge. The strong 100 KHz signals were generally a characteristic of fast charging. Another characteristic of fast charging is seen in Figure 39. This figure is a frequency vs. time spectrogram of the entire flight. The black

vertical lines that appear from 0 to 0.1 MHz seem to be associated with the fast charge.

Occasionally they appear in the ramped case, but infrequently.

VI. DATA ANALYSIS

For calculations in this chapter, the following notation is assigned:

N - Particle Density.

M - Mass of Ion.

m - Mass of Electron.

B - Magnetic Field Strength.

The table below is a list of constants that are used to calculate characteristic frequencies that would be expected in the ionosphere. The variation of the magnetic field during the flight is not strong enough to have a noticeable effect.

Table 4. Standard Constants.

Magnetic Field (B)	$3.20 \times 10^{-5} \cdot \text{tesla}$
Particle Density (nominal)	$5.00 \times 10^4 \cdot \text{cm}^{-3}$
Electron Mass (m)	$0.91 \times 10^{-30} \cdot \text{kg}$
Proton Mass (M)	$1.67 \times 10^{-27} \cdot \text{kg}$
Oxygen Mass	$2.67 \times 10^{-26} \cdot \text{kg}$
Helium Mass	$6.68 \times 10^{-27} \cdot \text{kg}$
ϵ_0	$8.854 \times 10^{-12} \cdot \frac{\text{farad}}{\text{meter}}$
q (Electron Charge)	$1.67 \times 10^{-19} \cdot \text{coul}$

The particles that are expected to generate frequencies in the ionosphere are the electron, proton, helium, and the oxygen ions. Using the values in the table we calculate the gyro frequencies:

$$f = \frac{qB}{2\pi M}$$

(4) Calculation of the Gyro Frequencies

Using the above equation where q is the charge of an electron mass and B is the magnetic field strength we arrive at the following nominal gyro frequencies:

Table 5. Gyro Frequencies

Electron	0.890 MHz
Proton	487.0 Hz
Helium	122.0 Hz
Oxygen	30.0 Hz

The plasma frequency is calculated by:

$$f = \sqrt{\frac{Nq^2}{\epsilon_0 M}} \cdot \frac{1}{2\pi}$$

(5) Calculation for Plasma Frequencies.

These calculated plasma frequencies of the particles in the plasma environment using a density of $5 \times 10^4 \text{ cm}^{-3}$, per the Wallops Digisonde, are:

Table 6. Plasma Frequencies

Electron	2.000 MHz
Proton	0.048 MHz
Helium	0.023 MHz
Oxygen	0.012 MHz

Figure 20 shows the densities obtained from the Wallops Digisonde and aboard the LP, and the associated range for plasma frequencies. The lower-hybrid frequency (LHR) is generally close to the geometric mean gyrofrequency:

$$\frac{1}{\omega_{LHR}^2} = \frac{1}{\Omega_e^2 \omega_c^2} + \frac{1}{\Omega_p^2}, \text{ where } \omega_c = \frac{qB}{M}, \text{ and } \Omega_p = \sqrt{\frac{Nq^2}{\epsilon_0 M}}$$

(6) Lower Hybrid Frequency.

If $\Omega_e \omega_c \ll \Omega_p^2$, then $\omega_{LHR} \sim \Omega_e \omega_c$, and $f_{LHR} \sim f_{gmf}$. Where f_{gmf} , the geometric mean gyrofrequency, is defined as:

$$f_{gmf} = \frac{\sqrt{q^2 B^2}}{M \cdot m} \cdot \frac{1}{2\pi}$$

(7) Geometric Mean Gyrofrequency.

Assuming the following masses, the LHR frequencies are:

Table 7. Lower Hybrid Frequencies

Proton	20.9 KHz
Helium	10.5 KHz
Oxygen	5.2 KHz

The last wave that is possible is the electrostatic ion sound wave. To calculate this we first find the ion sound velocity. Assuming one dimensional compression, $\gamma = 1$, we have:

$$V_s = \sqrt{\frac{kT + \gamma kT}{M}} \quad \text{where} \quad V_s = 620 \frac{m}{src}$$

(8) Ion Sound Velocity.

Using this velocity of the sound wave we calculate the electrostatic ion sound wave frequency to be:

$$f = \sqrt{f_p^2 + k^2 V_s^2} \cdot \frac{1}{2\pi}$$

(9) Electrostatic Ion Wave

Assuming a wavelength of ~3 meters, a reasonable bound on the sheath size, we find a frequency in the range of .6 MHz.

The floating probe data were previously analyzed using standard fourier transform technique. Signals at 4 and 8 kilohertz (see Figure 27) were observed continuously during

the entire flight. The constant frequency suggests that these signals should be considered to be locally generated artifacts. There was one additional monochromatic signal beginning at 6 KHz at 100 seconds, rising monotonically to 9.3 KHz at 500 seconds. These variations do not correspond to any obvious physical parameters such as magnetic field strength or orientation, electron density, or altitude. This signal is therefore tentatively identified as an artifact. In addition to the three mentioned signals there was a broadband signal, produced during all discharge sequences, in the 0-2 KHz frequency range.. Note that the band pass filters previously shown in Figure 14 limits the sensitivity at the higher end of the transformation. The thermionic emitter operations generated narrow interference lines at ~2300 Hz, ~4500 Hz, ~6800 Hz, and ~8000 Hz.

There was no noticeable effect in the floating probe data that would have been in the range of the ion cyclotron frequencies that are dependent on the magnetic field. The lack of any signal may infer that either the signals were masked by noise, or some other phenomenon was taking place that did not allow signal detection.

The above calculations show that the lower hybrid frequency falls within the range of what was observed in the skin current probe at 100 KHz. Also shown in the calculations is the electrostatic ion sound wave. If we restrict the dimensions of the plasma sheath then it may be possible to generate the electrostatic ion sound wave. If such a wave is generated it would fall in the same range of the lower hybrid and would be difficult to detect. The author does not classify the signals as lower hybrid or electrostatic, but notes that those types of waves could generate the signals observed in the data.

The skin current probe yielded the high-frequency data that appears to harbor frequencies of interest. The analysis of the data was similar to that of the floating probe. The signals of the probe vary with events of the flight, but this may not be due to any of the grounding techniques.

The three orientations in the magnetic field did not have any apparent effect on any of the data analyzed.

VII. CONCLUSION

The SPEAR III data has not been fully explored. There are opportunities to explore many aspects of it. The finding of waves that may be the lower hybrid or electrostatic, warrants further investigation into the mechanism of their generation. The association these waves may have to one of the grounding experiments needs further study. A more detailed analysis is needed on the ESA data to understand the mechanism of the large flux in the low energy range. The finding of characteristic frequency in the range of the lower hybrid, and possibly electrostatic ion sound wave, may be the key to solving the spacecraft charging problem.

The ESA were extremely useful for this analysis. The frequency ranges of the floating probe were too low to be of significant use. The skin current probe revealed a characteristic 100 KHz signal.

The success of this flight clearly demonstrates that current theory and engineering is capable of achieving the objectives of the sponsor. Engineers were capable of developing the hardware and demonstrated its survivability in the plasma chamber. The success and robustness of both SPEAR I and SPEAR III flights may be attributed to rigorous testing done at the NASA-Plum Brook B-2 chamber and the space chamber at the University of Maryland. All future space experiments would benefit from this type of testing prior to launch.

APPENDIX A: COLLECTED ILLUSTRATIONS

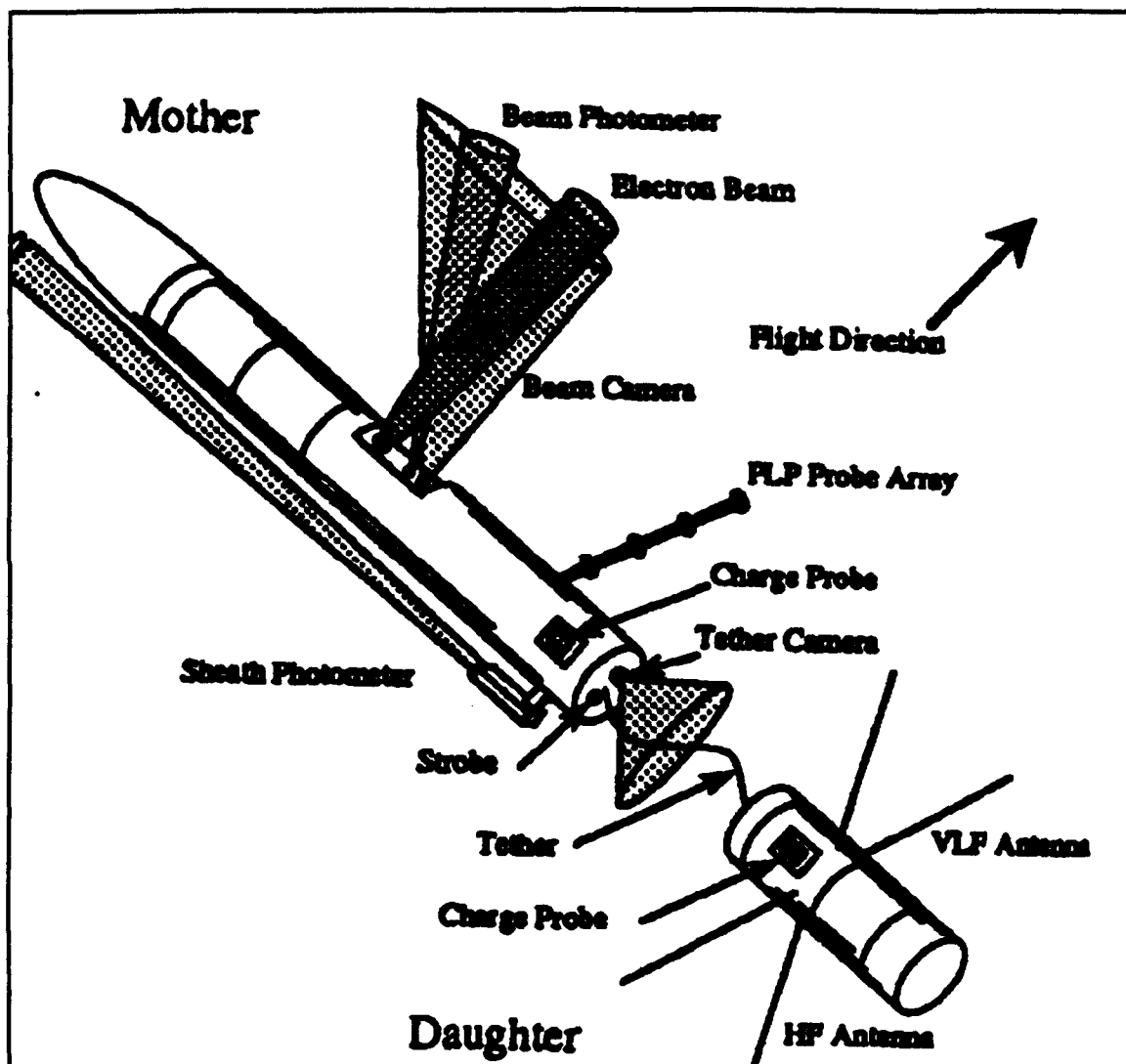


Figure 1. Charge II.

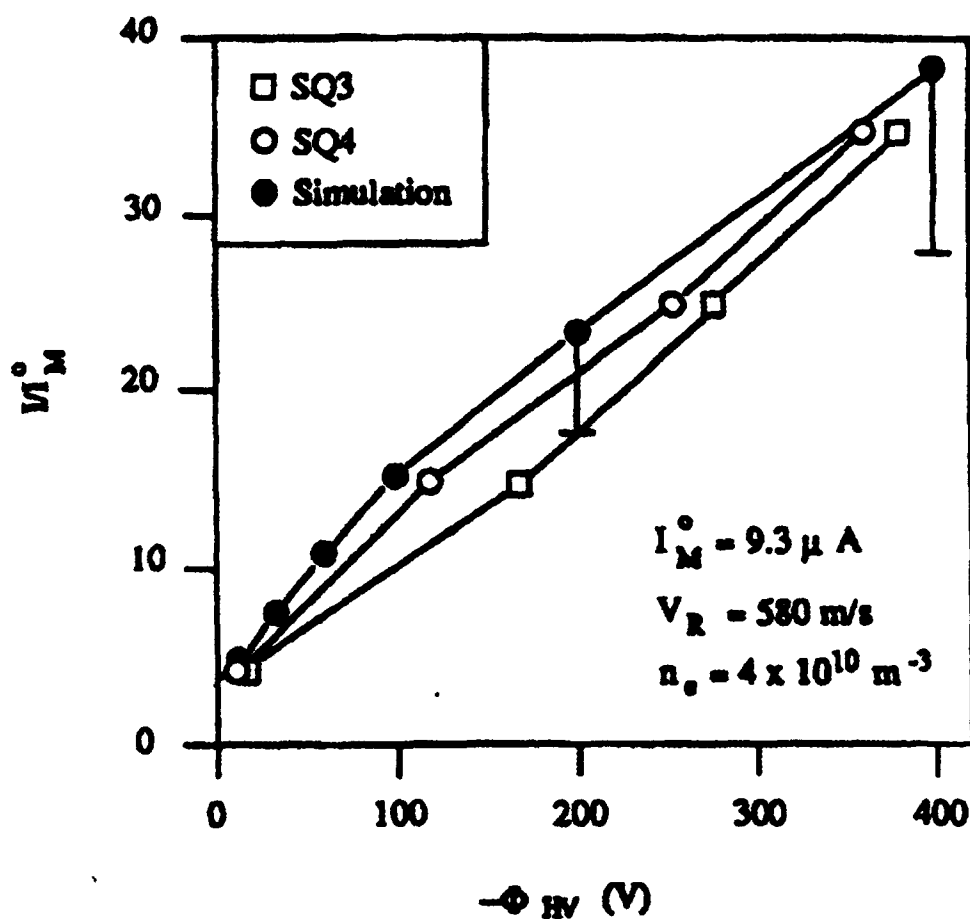


Figure 2. Charge II I-V Curve.

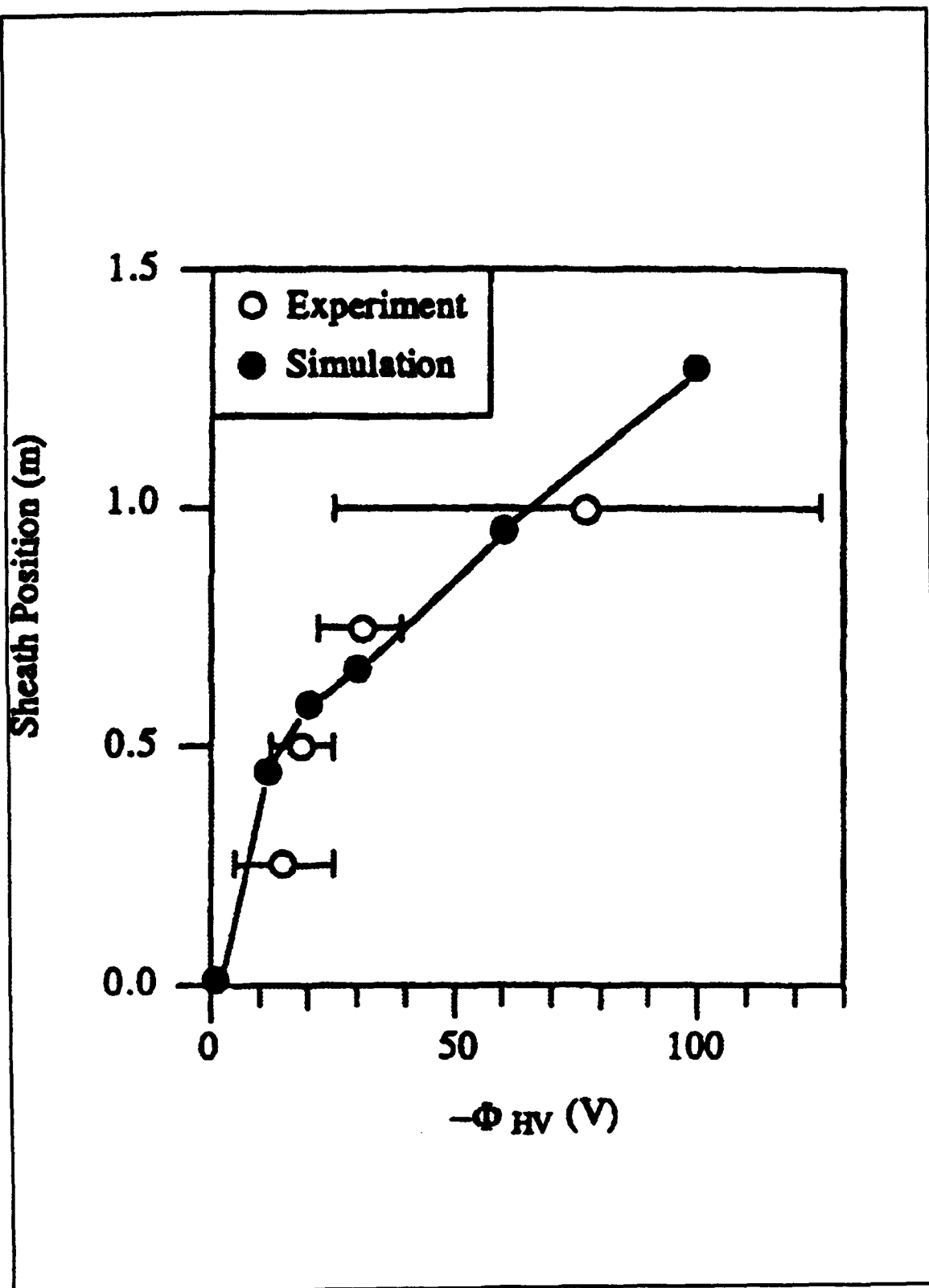


Figure 3. Charge II Sheath Position.

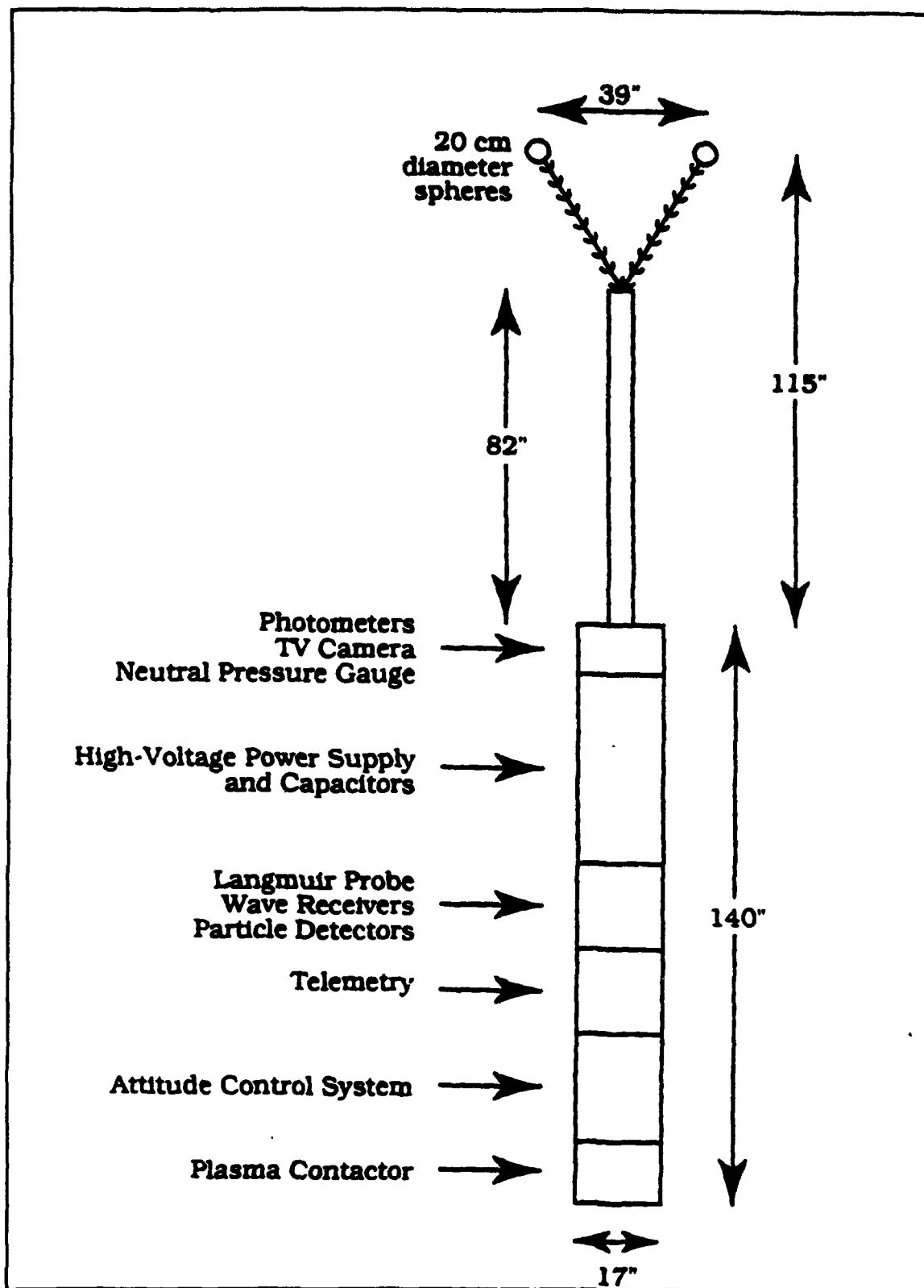
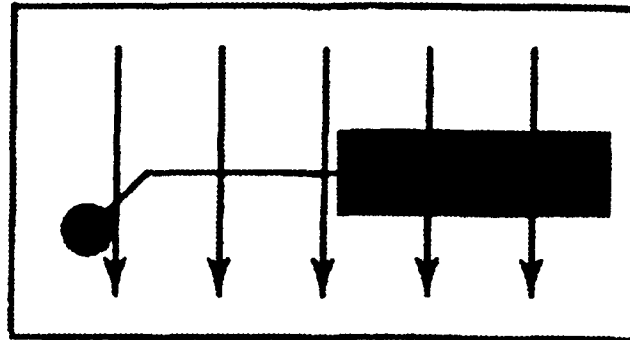
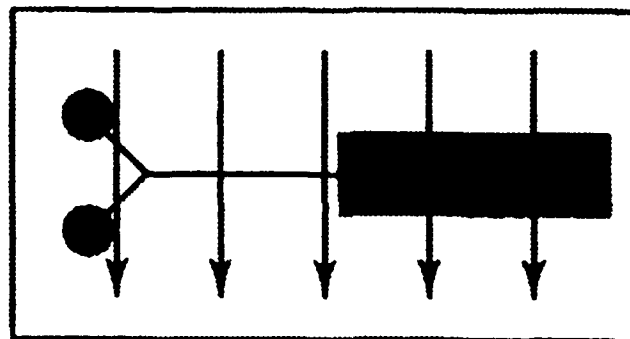


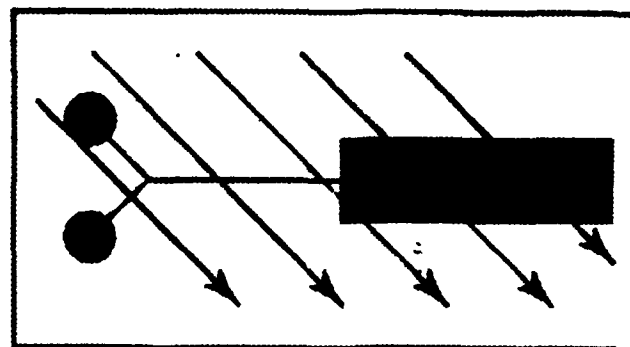
Figure 4. SPEAR I Rocket Configuration



Position 1. Near Perpendicular



Position 2. V-Plane of Booms Parallel



Position 3. Boom of Sphere 1 Parallel

Figure 5. Magnetic Field Orientation.

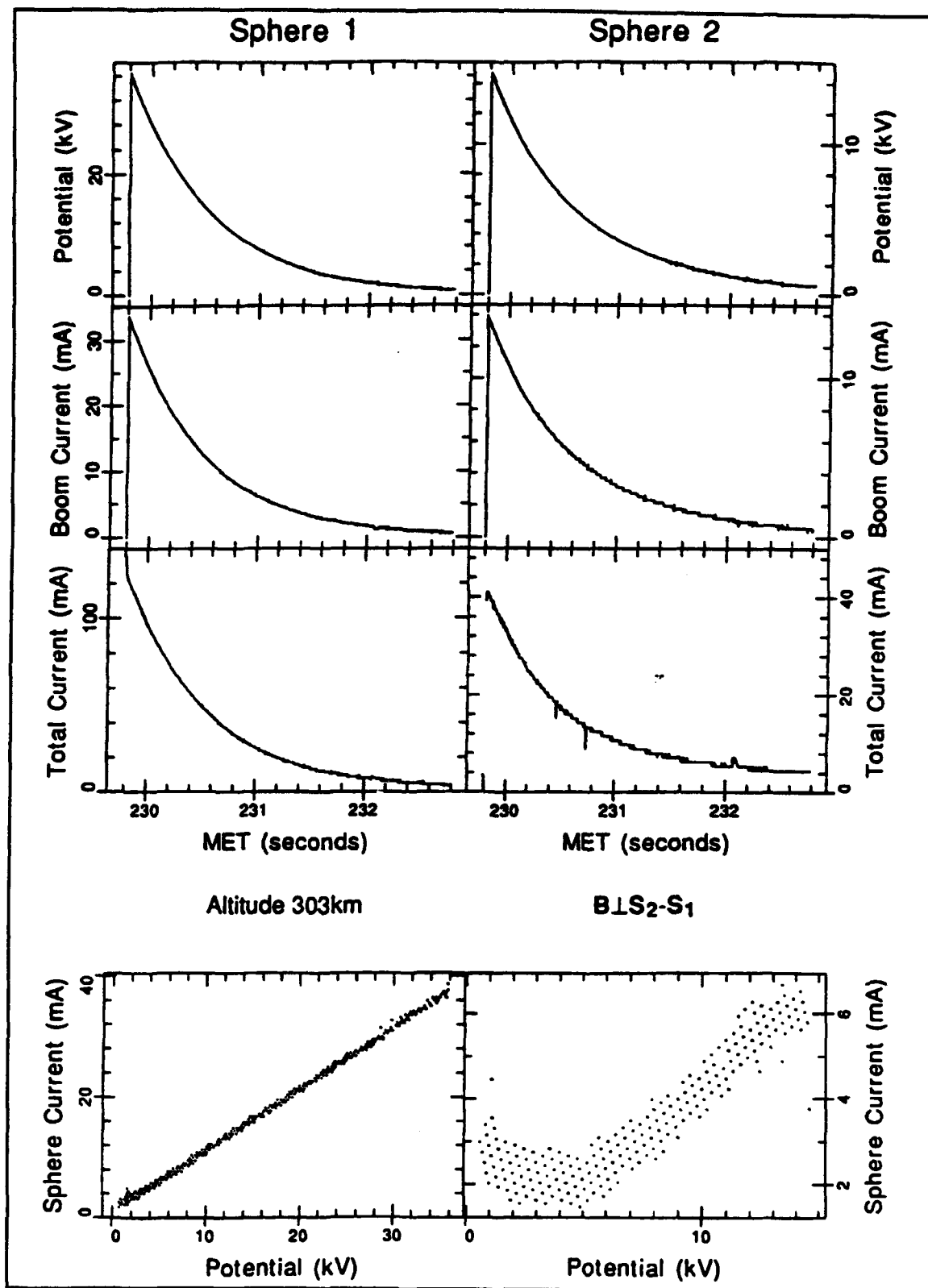


Figure 6. SPEAR I Current Potentials.

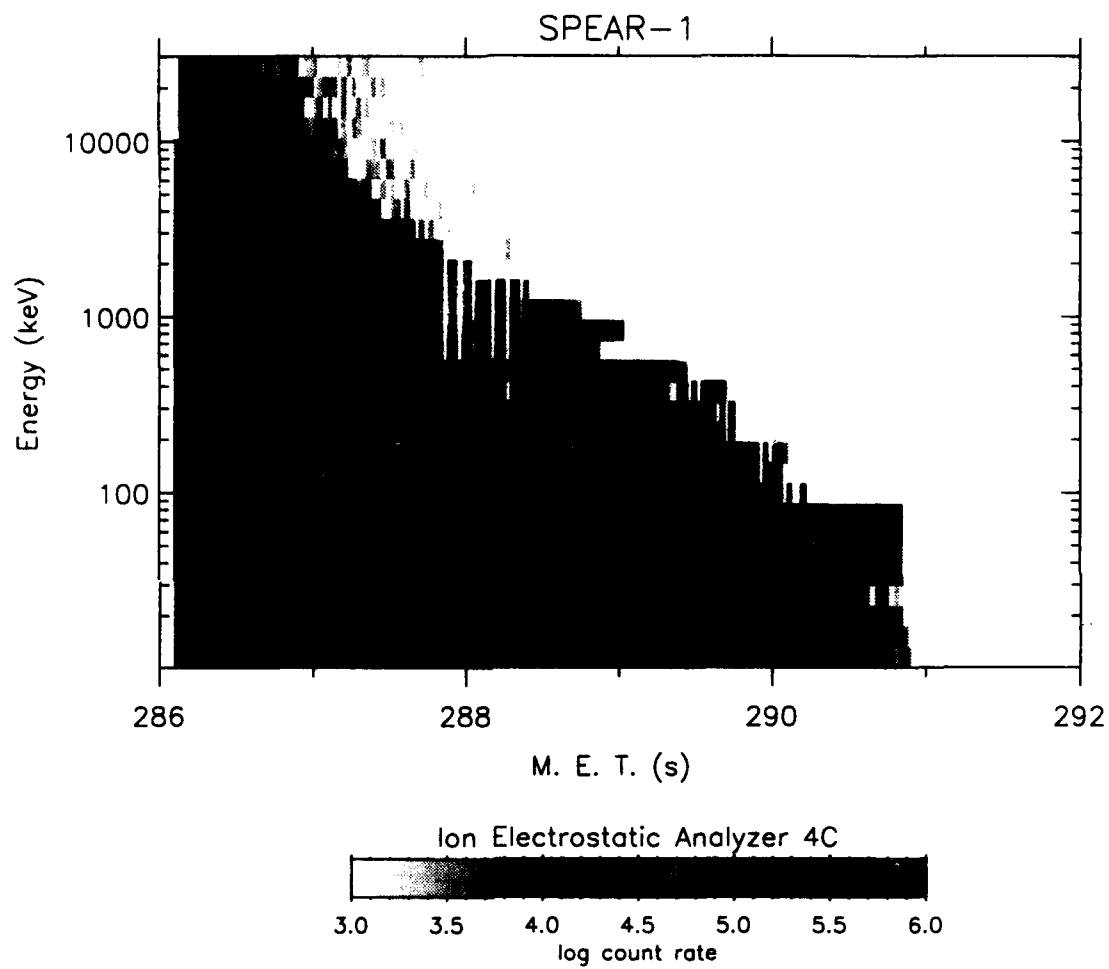


Figure 7. SPEAR I ESA.

SPEAR III CRITICAL DESIGN REVIEW

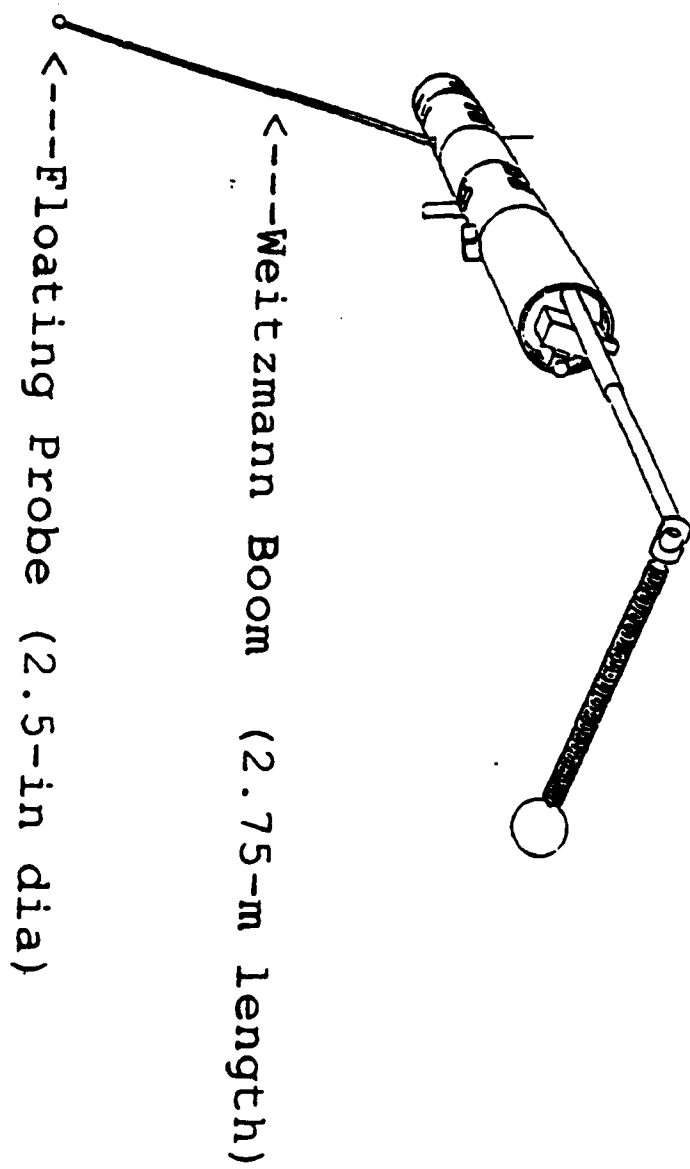


Figure 8. SPEAR III Configuration.

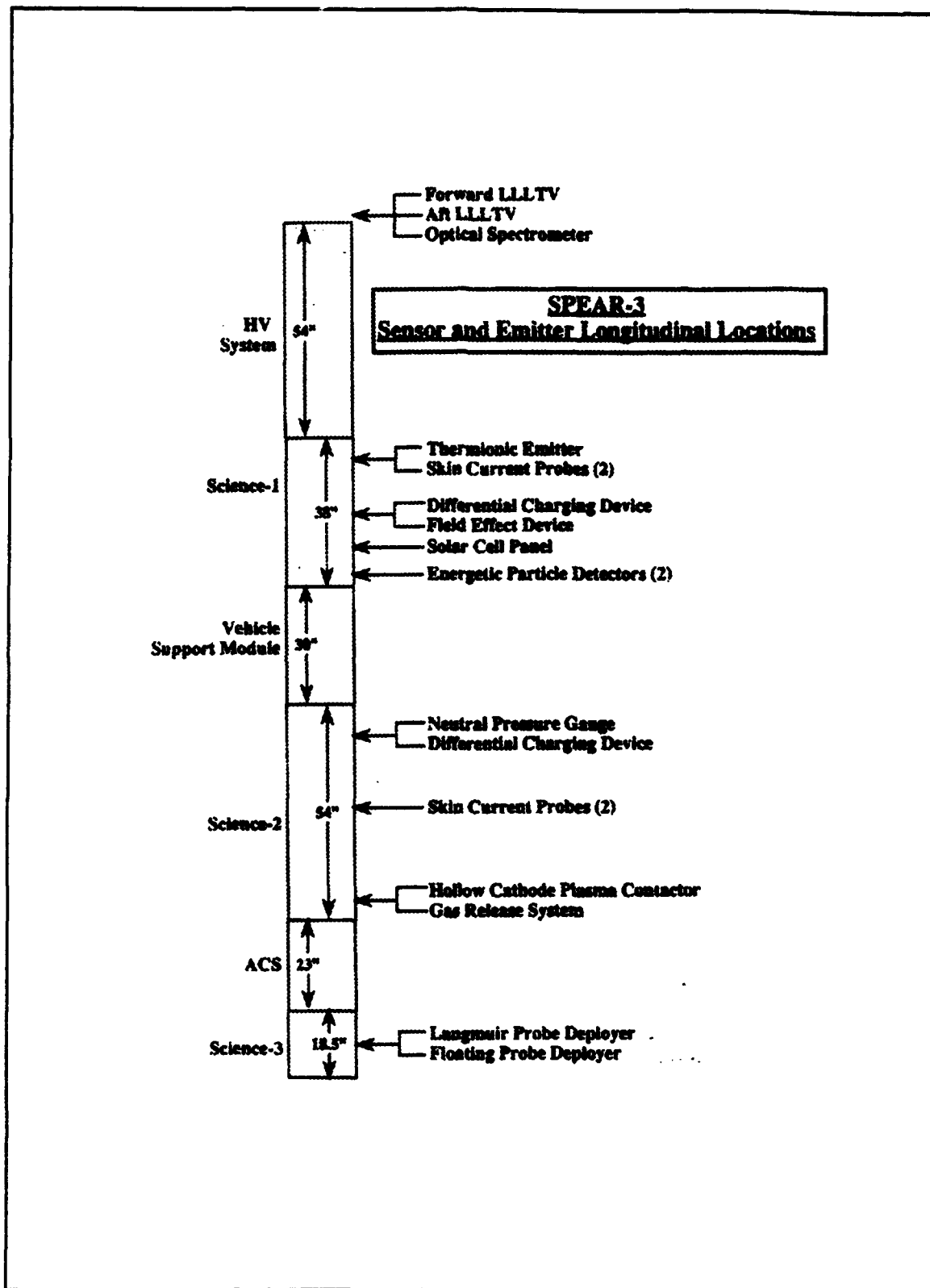


Figure 9. Sensor and Emitter Longitudinal Locations.

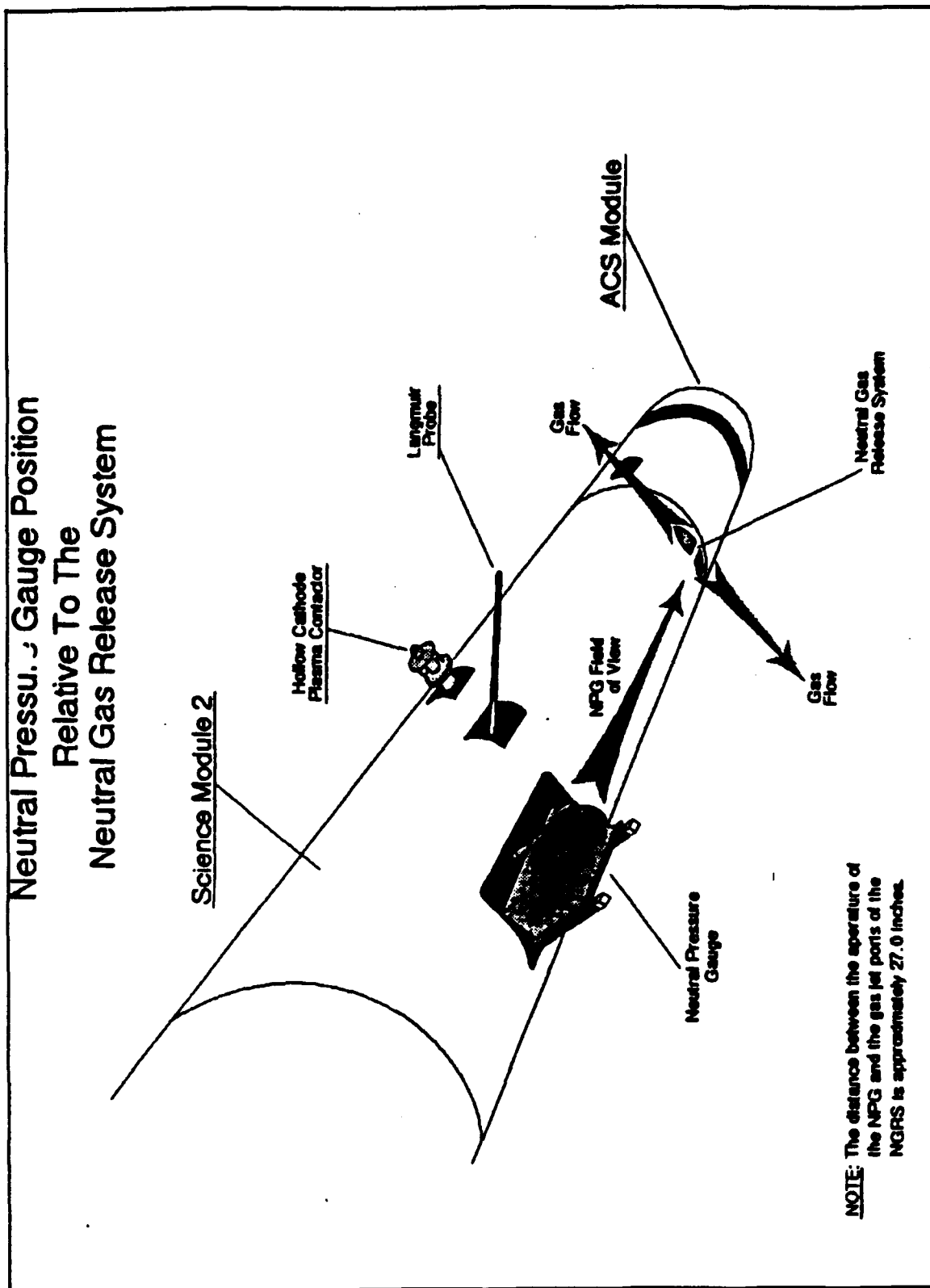


Figure 10. Neutral Pressure Gauge Position.



SPEAR-3 Sensor and Emitter Orientations

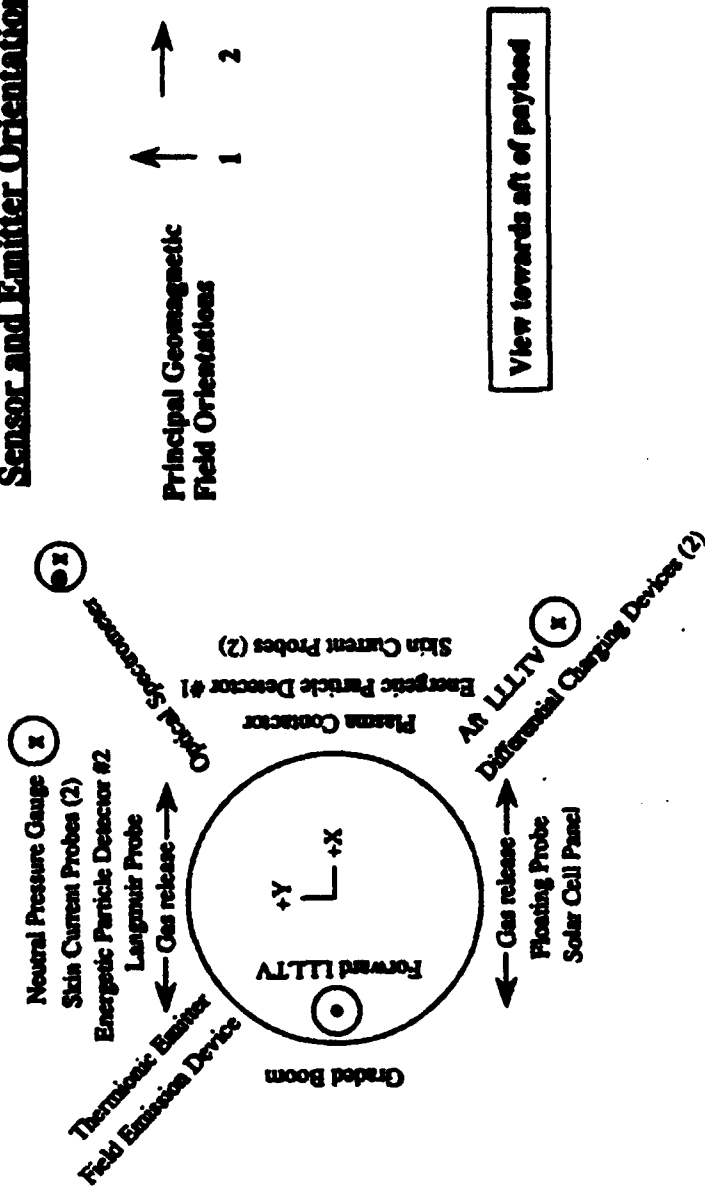
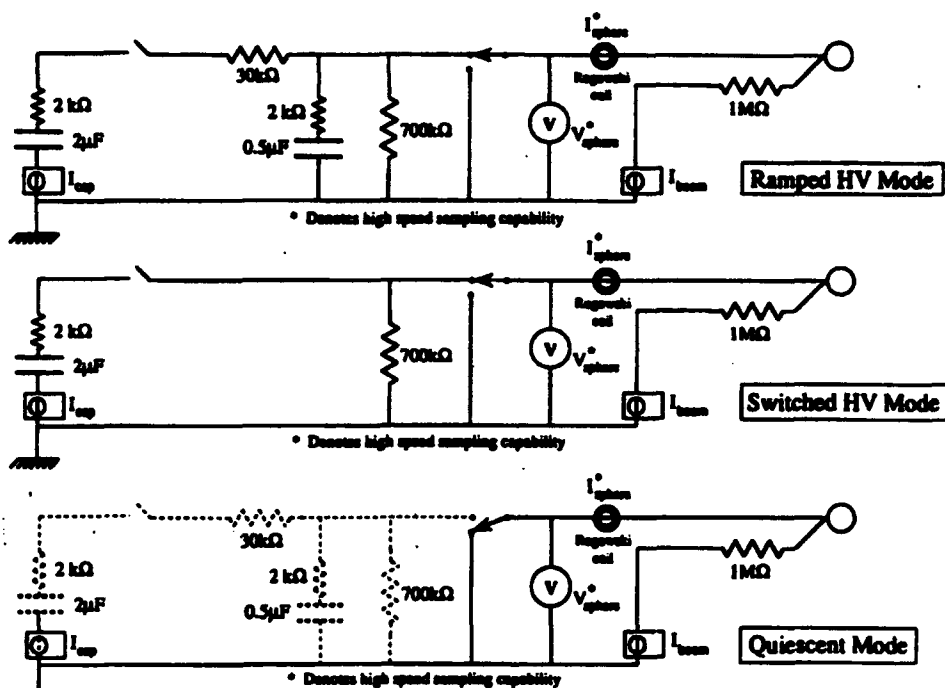


Figure 11. Sensor and Emitter Orientations.



SPEAR-3 SCIENCE MEETING, W. J. SCHAFER ASSOC., ARLINGTON VA AUG 6-7 1981
 CENTER FOR ATMOSPHERIC AND SPACE SCIENCES UTAH STATE UNIVERSITY



Simplified Schematic Diagrams of HV Capacitor Discharge Modes and Quiescent Mode

Figure 12. Schematic of HV Capacitor Discharge Modes/Quiescent Mode.

SPEAR III **TIMING OF HIGH-SPEED DATA SYSTEM**

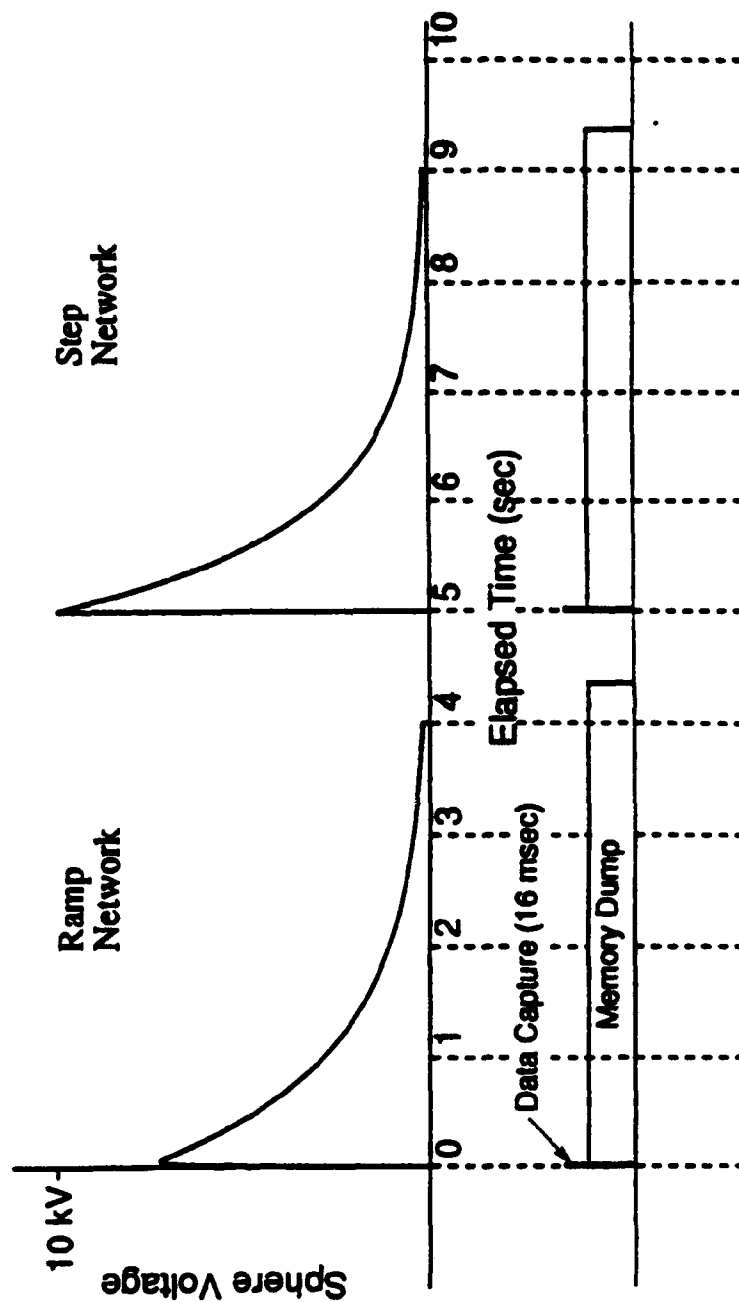


Figure 13. SPEAR III Timing of High-speed Data System.

SPEAR-III Simplified High-Speed Data Schematic

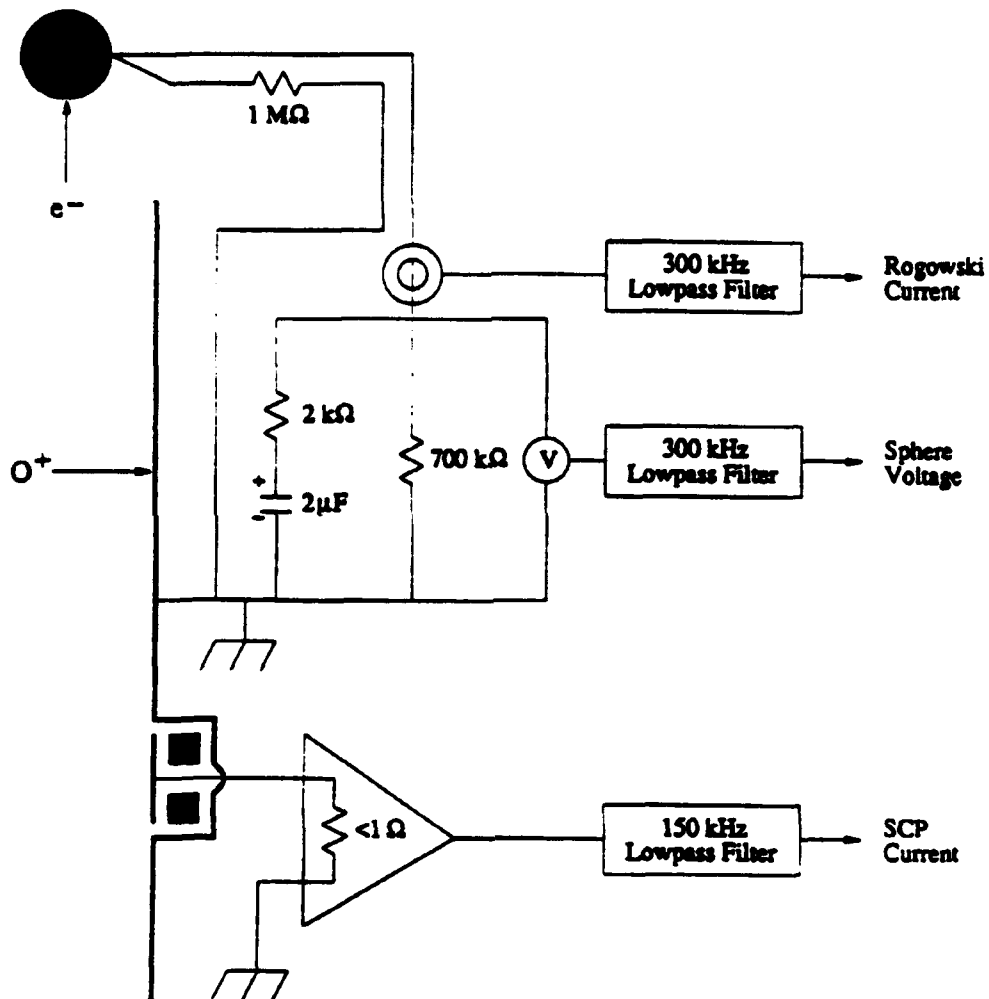


Figure 14. Simplified High-speed Data Schematic.

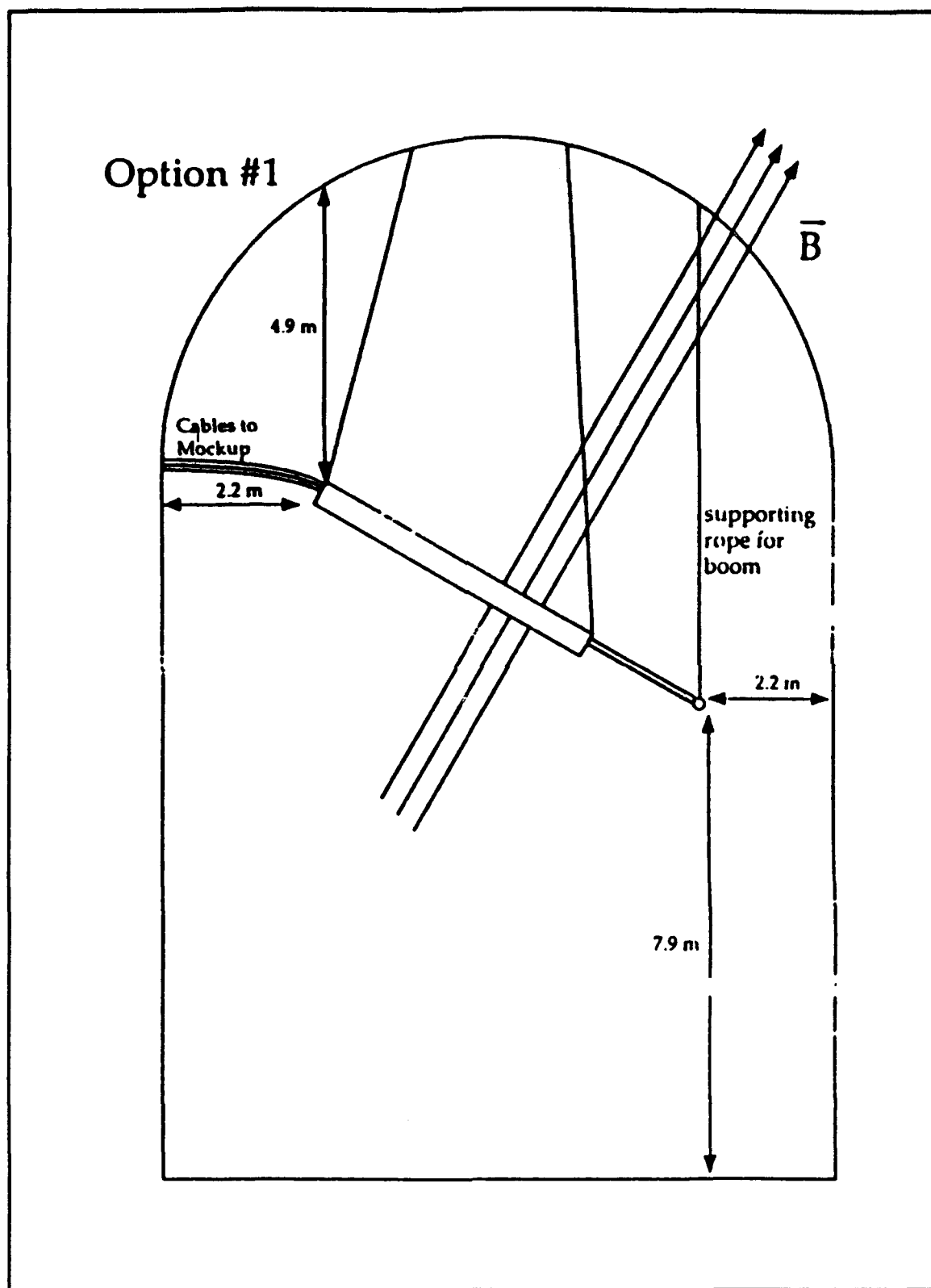


Figure 15. Plum Brook Plasma Chamber.

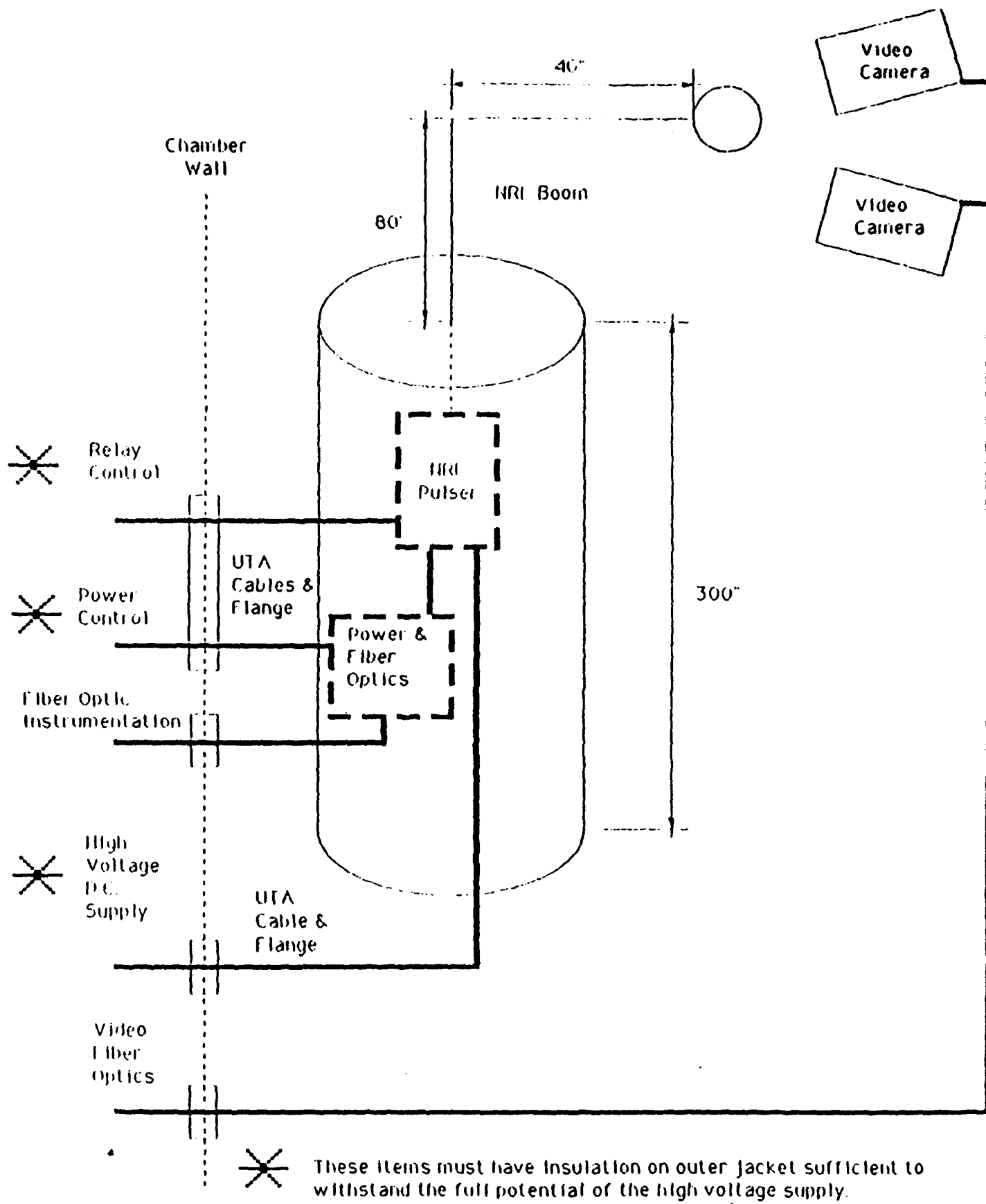


Figure 16. Mockup Physical Configuration.

Suspension of the Mockup

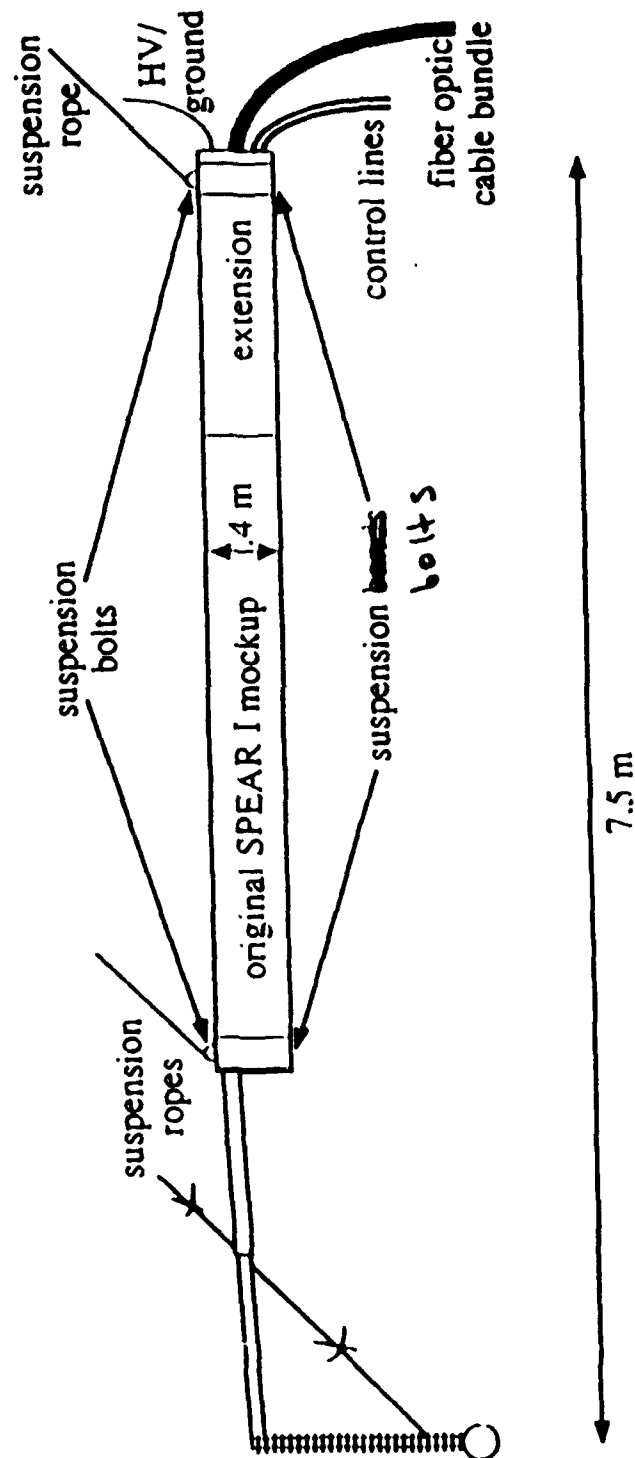


Figure 17. Plum Brook Chamber Suspension.

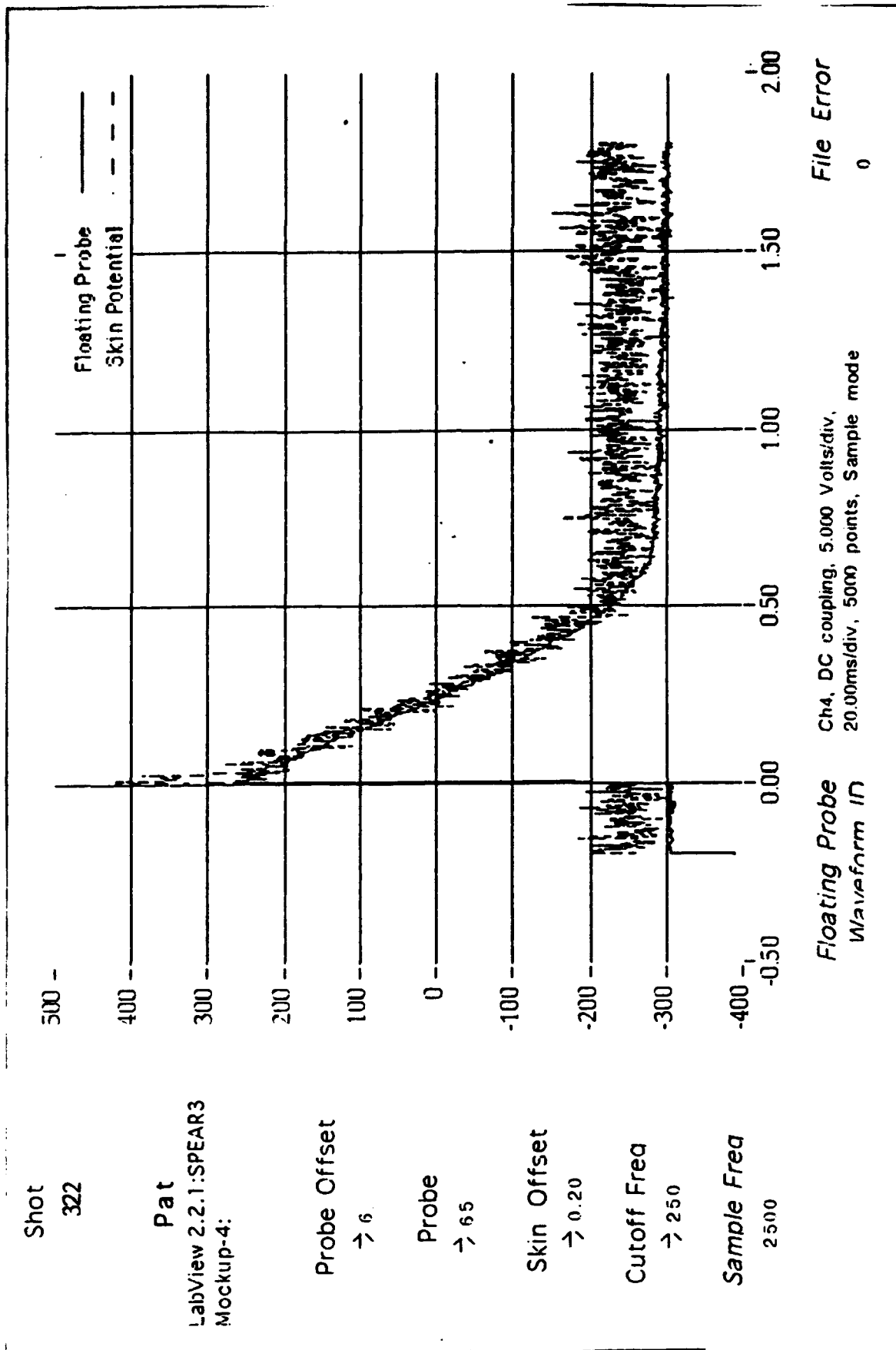


Figure 18. Floating Probe Waveform - Shot 322

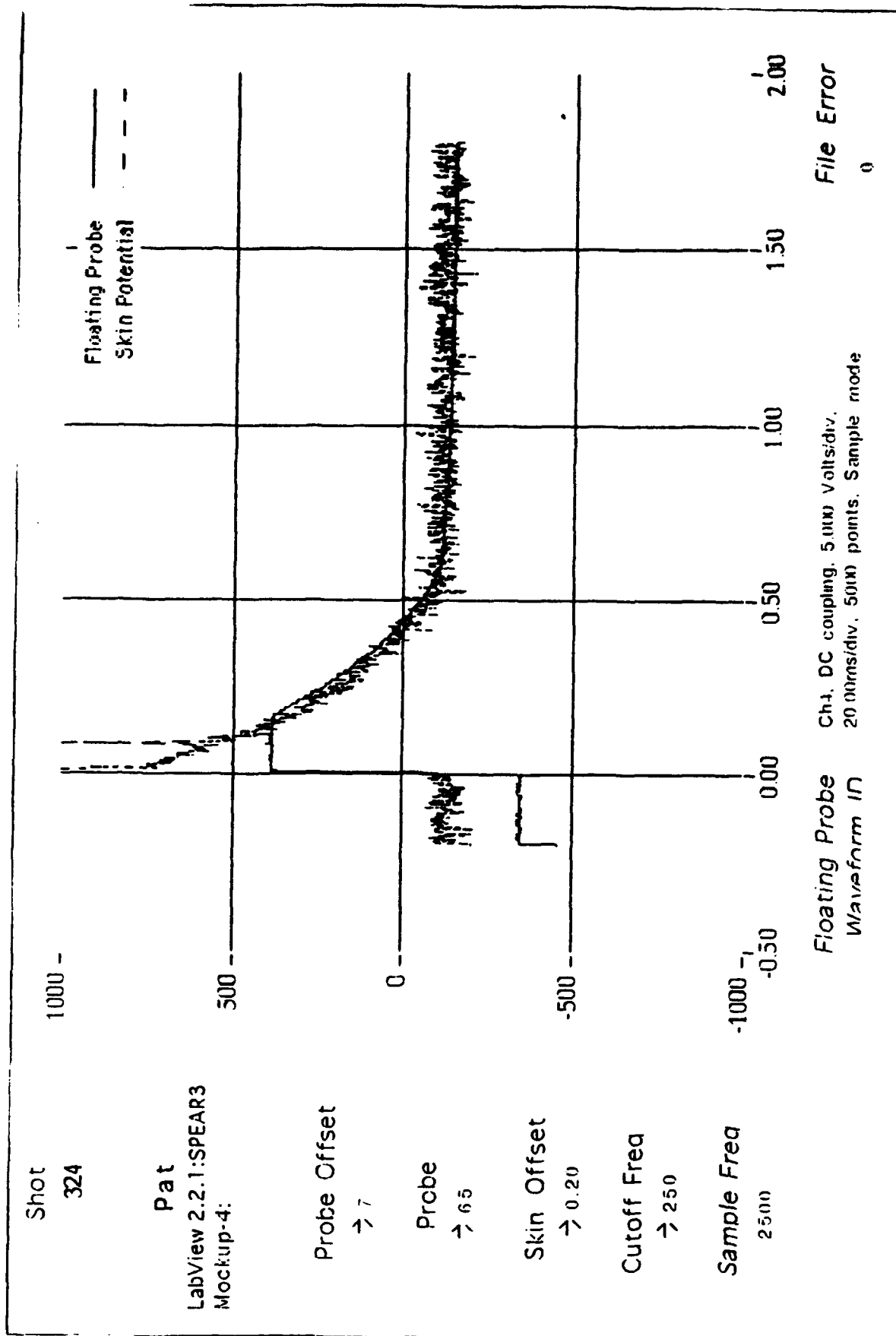


Figure 19. Floating Probe Waveform - Shot 324.

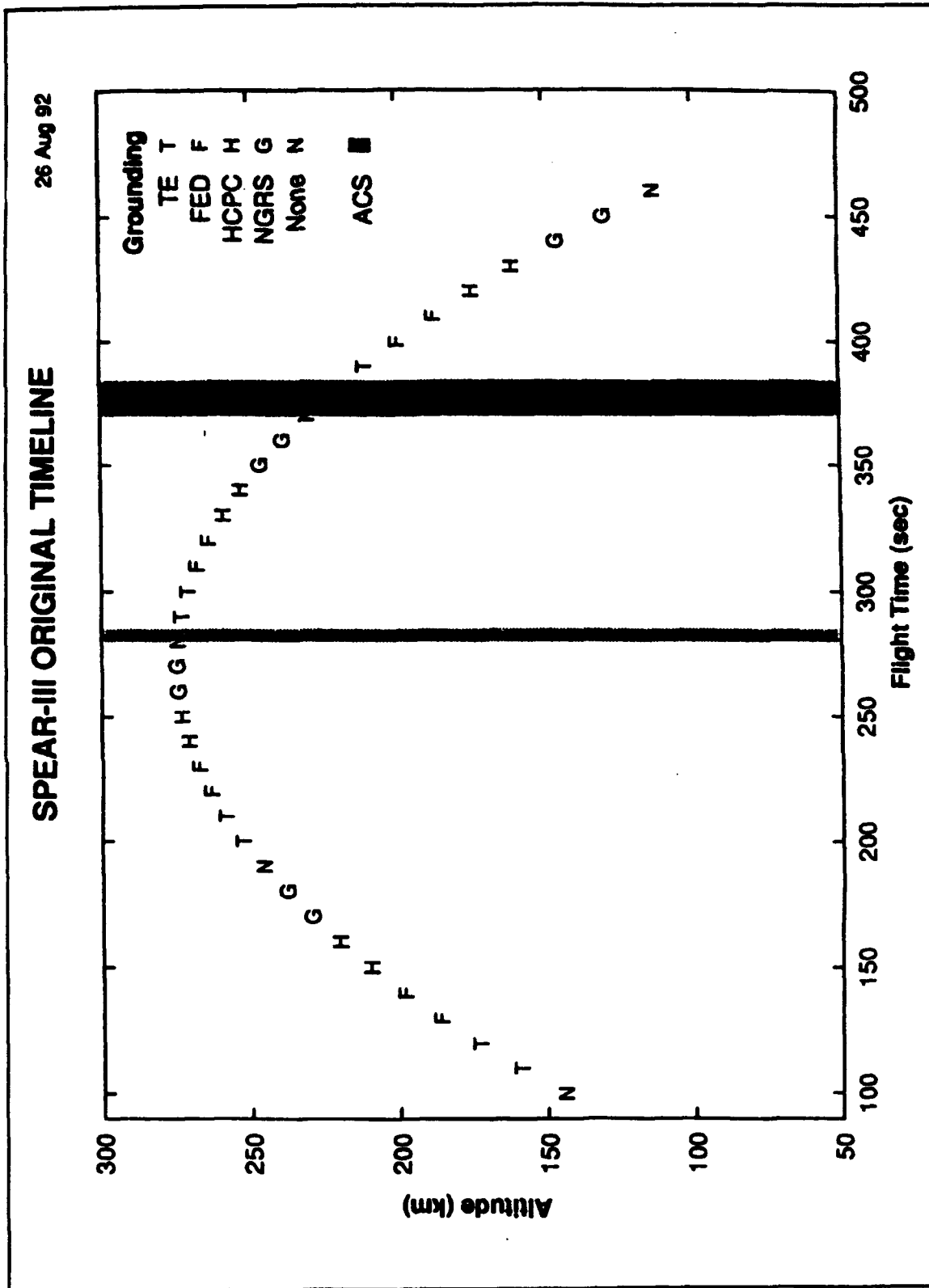


Figure 20. SPEAR III Original Timeline.

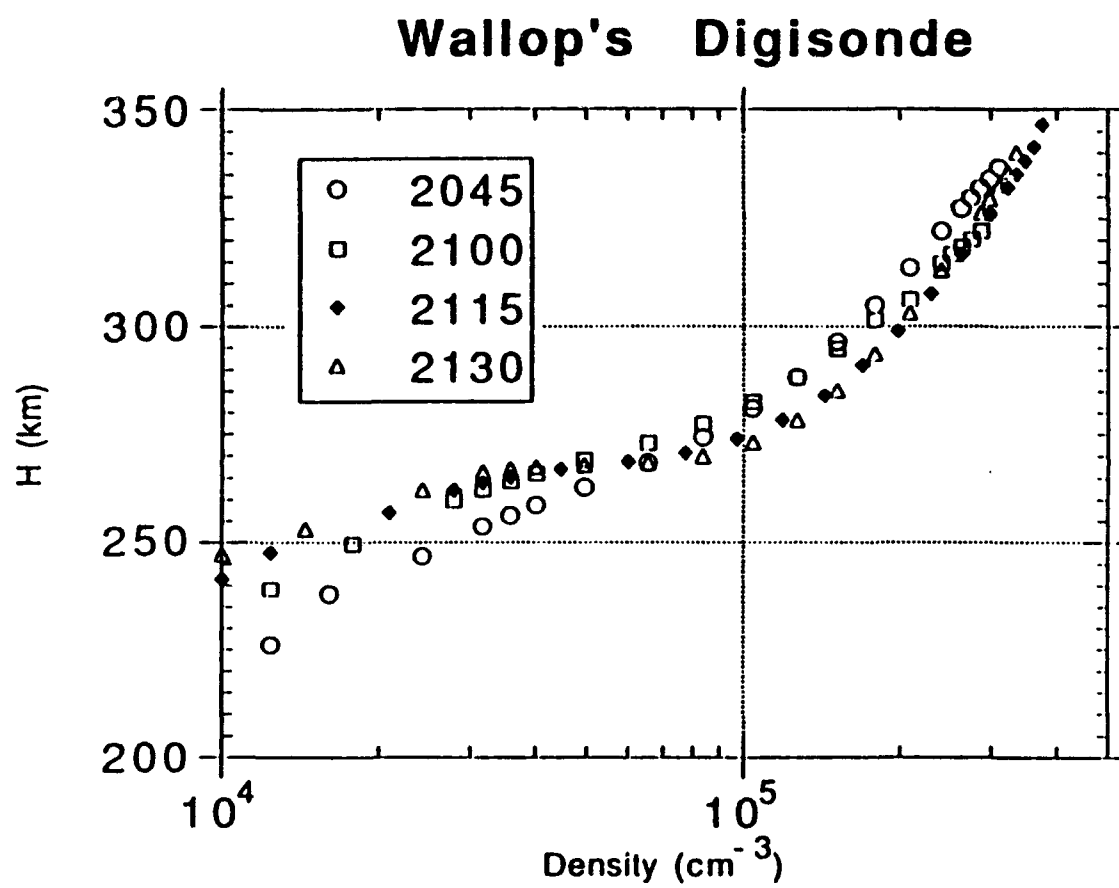


Figure 21. Wallop's Digisonde.

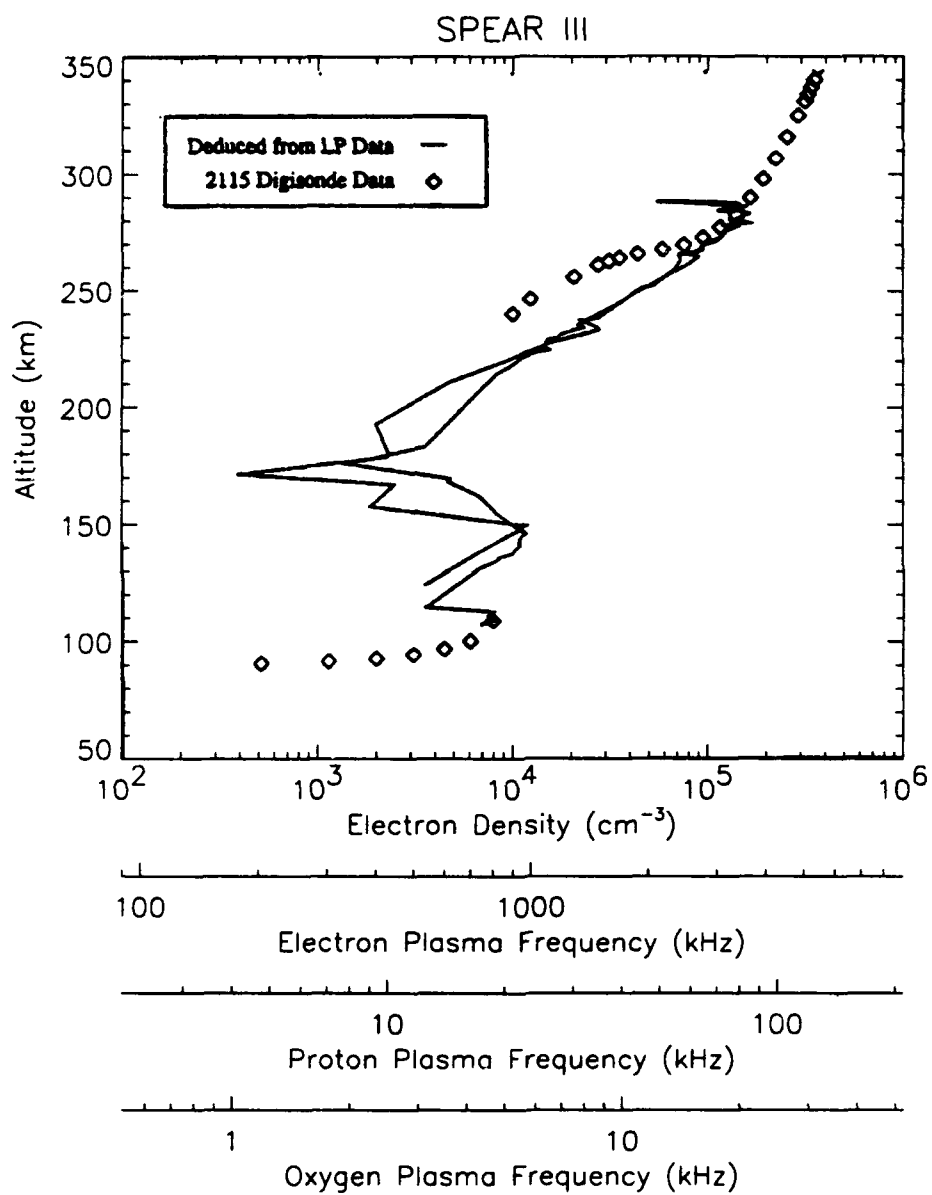


Figure 22. SPEAR III Electron Density.

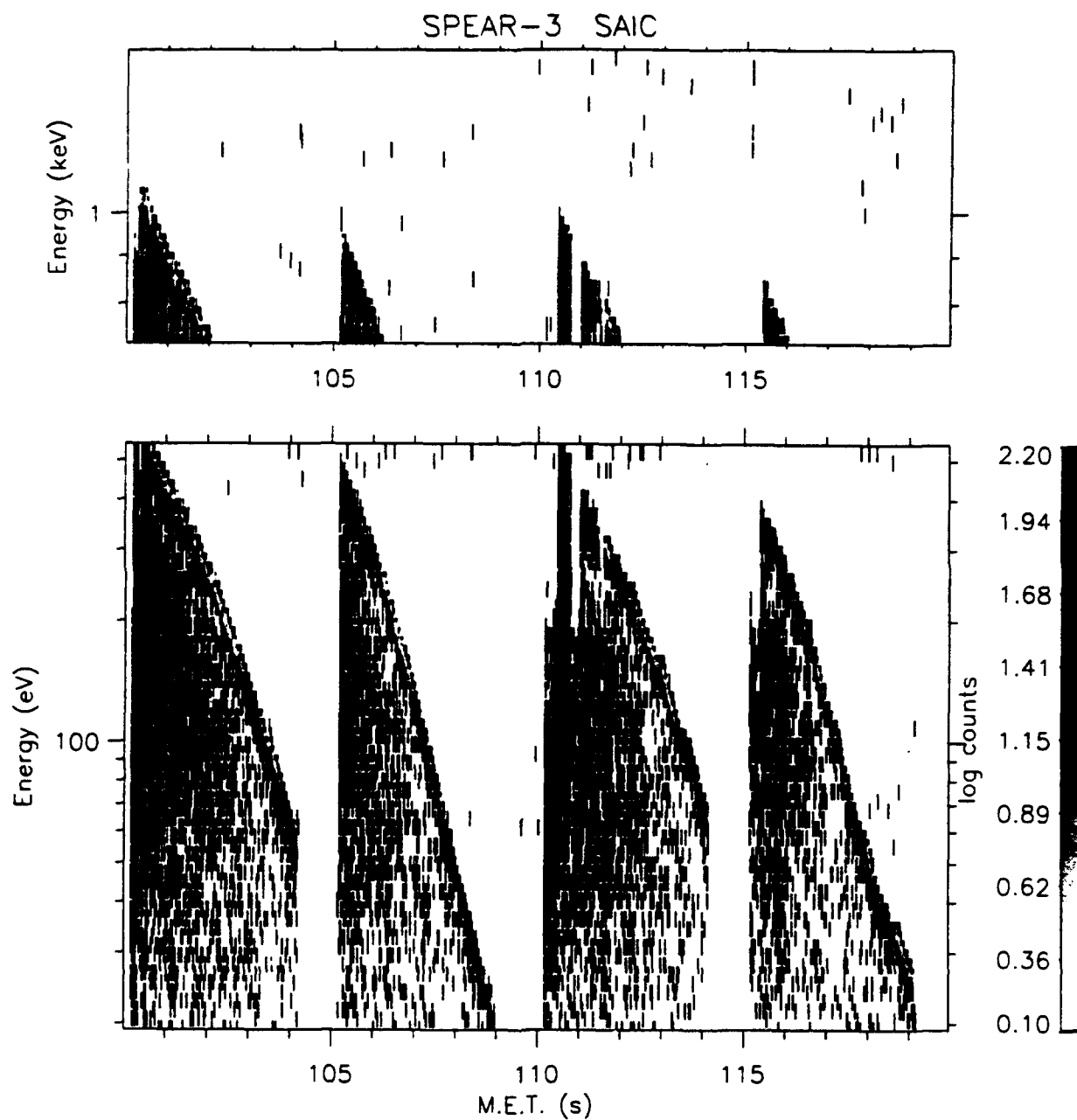


Figure 23. SPEAR III SAIC - 100 Seconds.

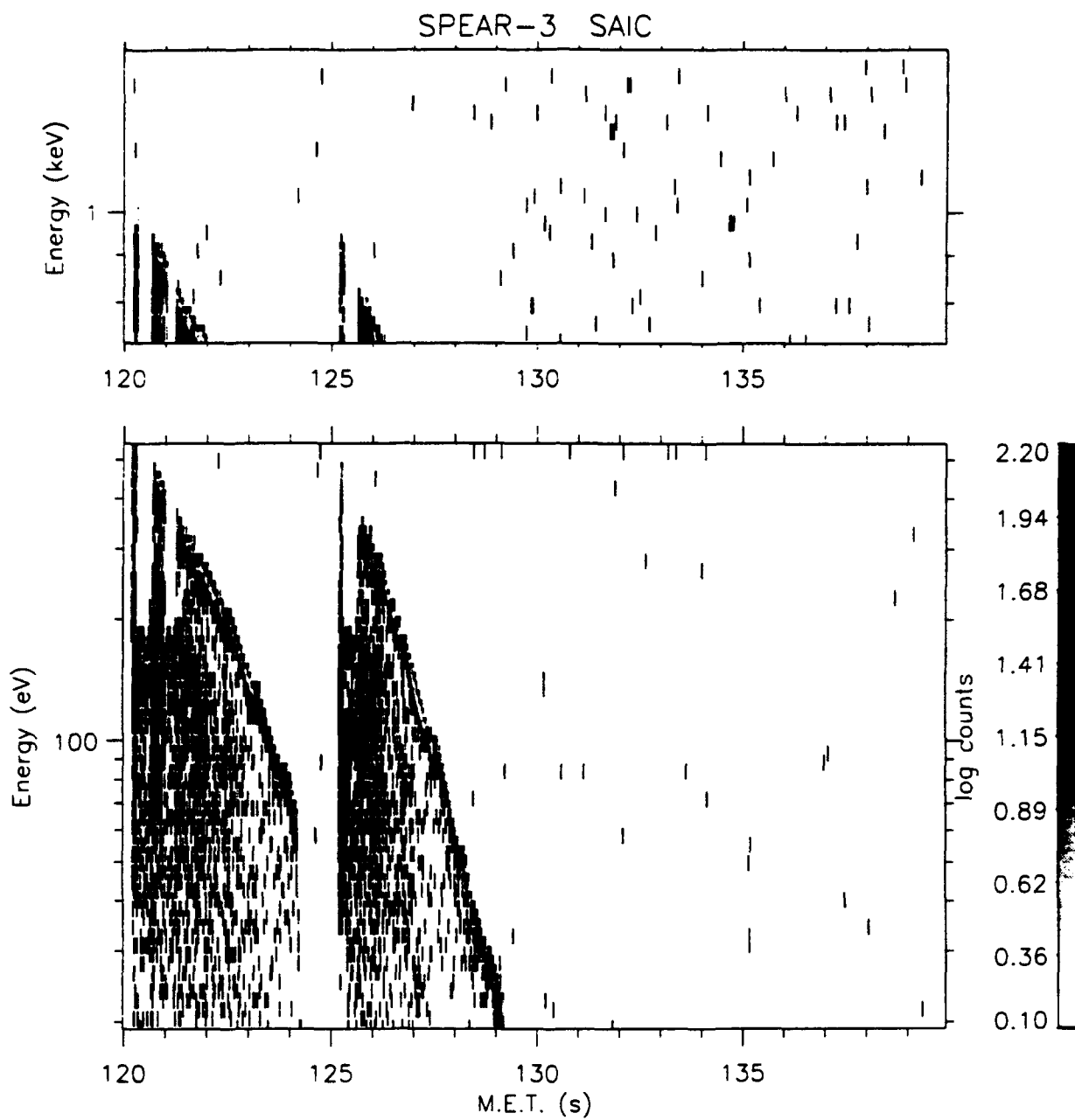


Figure 24. SPEAR III SAIC - 120 Seconds.

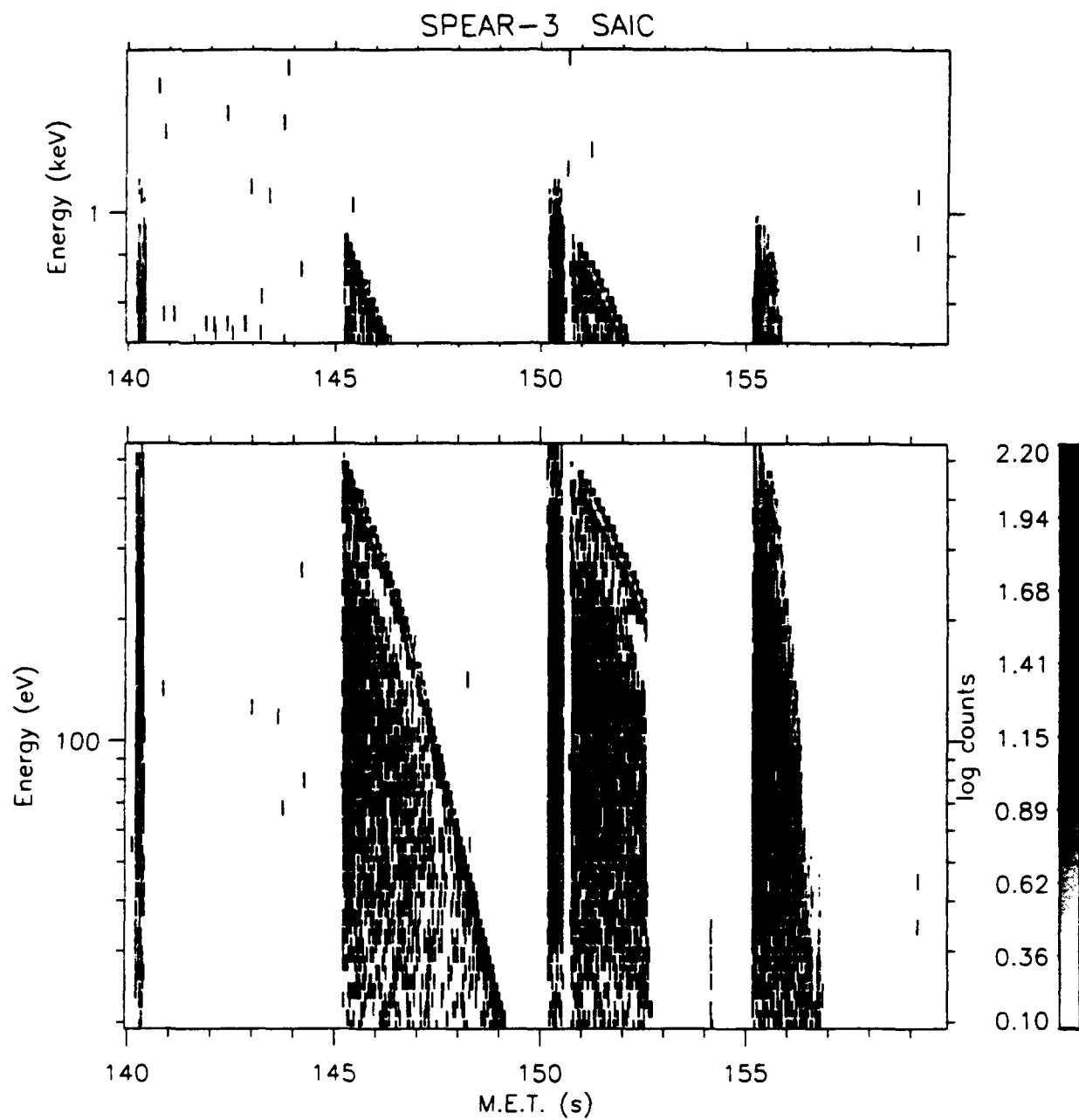


Figure 25. SPEAR III SAIC - 140 Seconds.

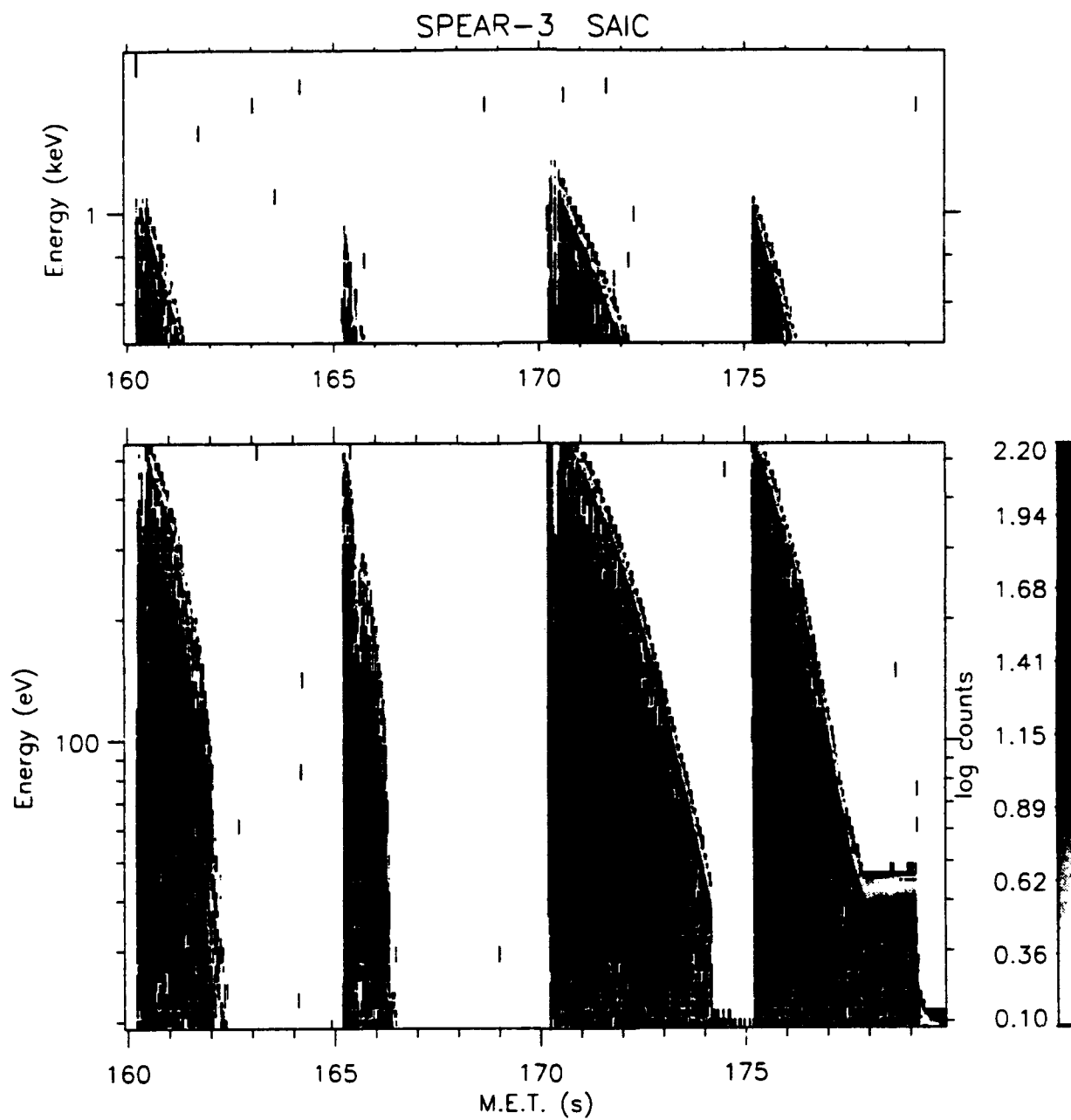


Figure 26. SPEAR III SAIC - 160 Seconds.

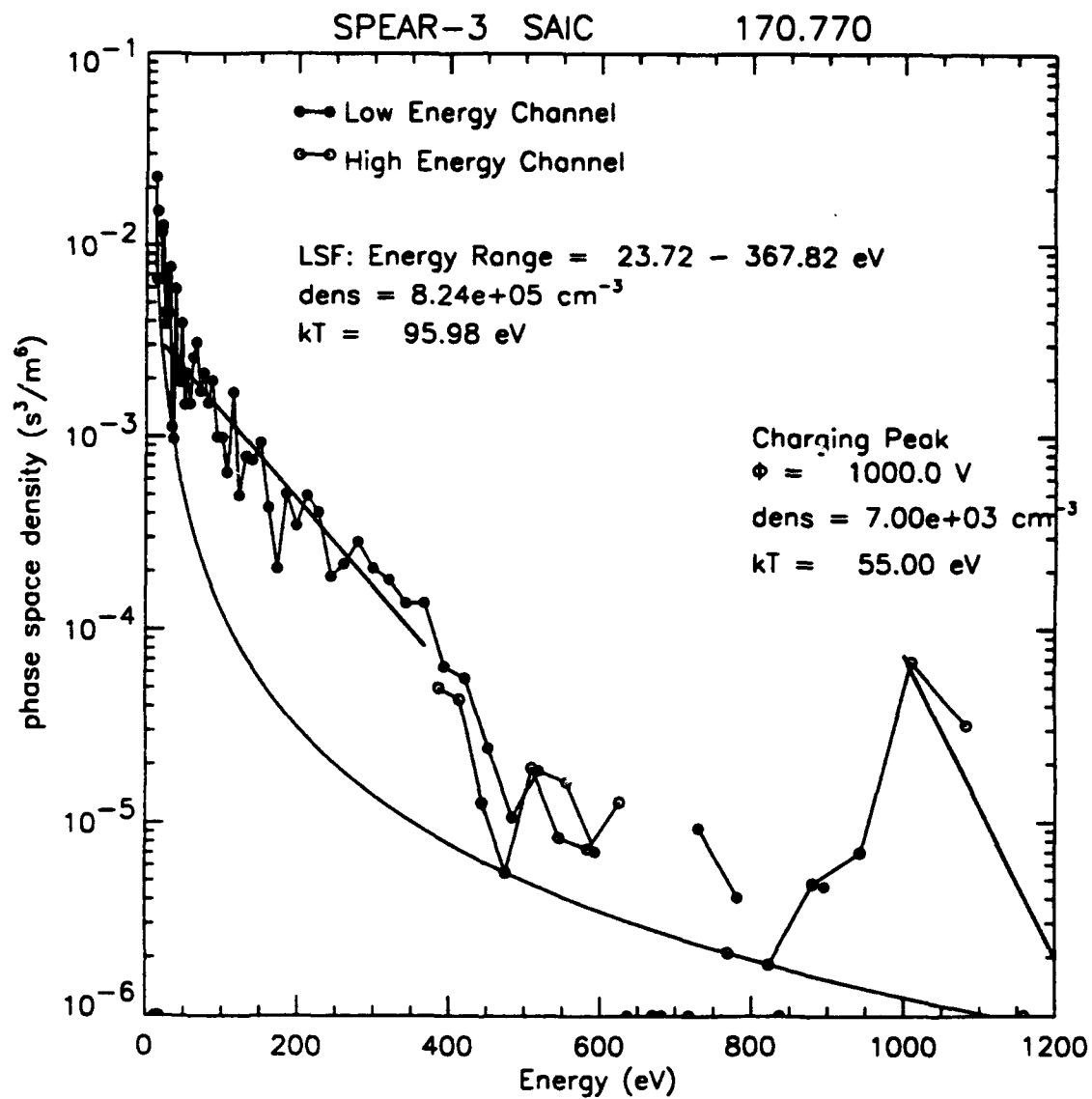


Figure 27. SPEAR III SAIC 170.770.

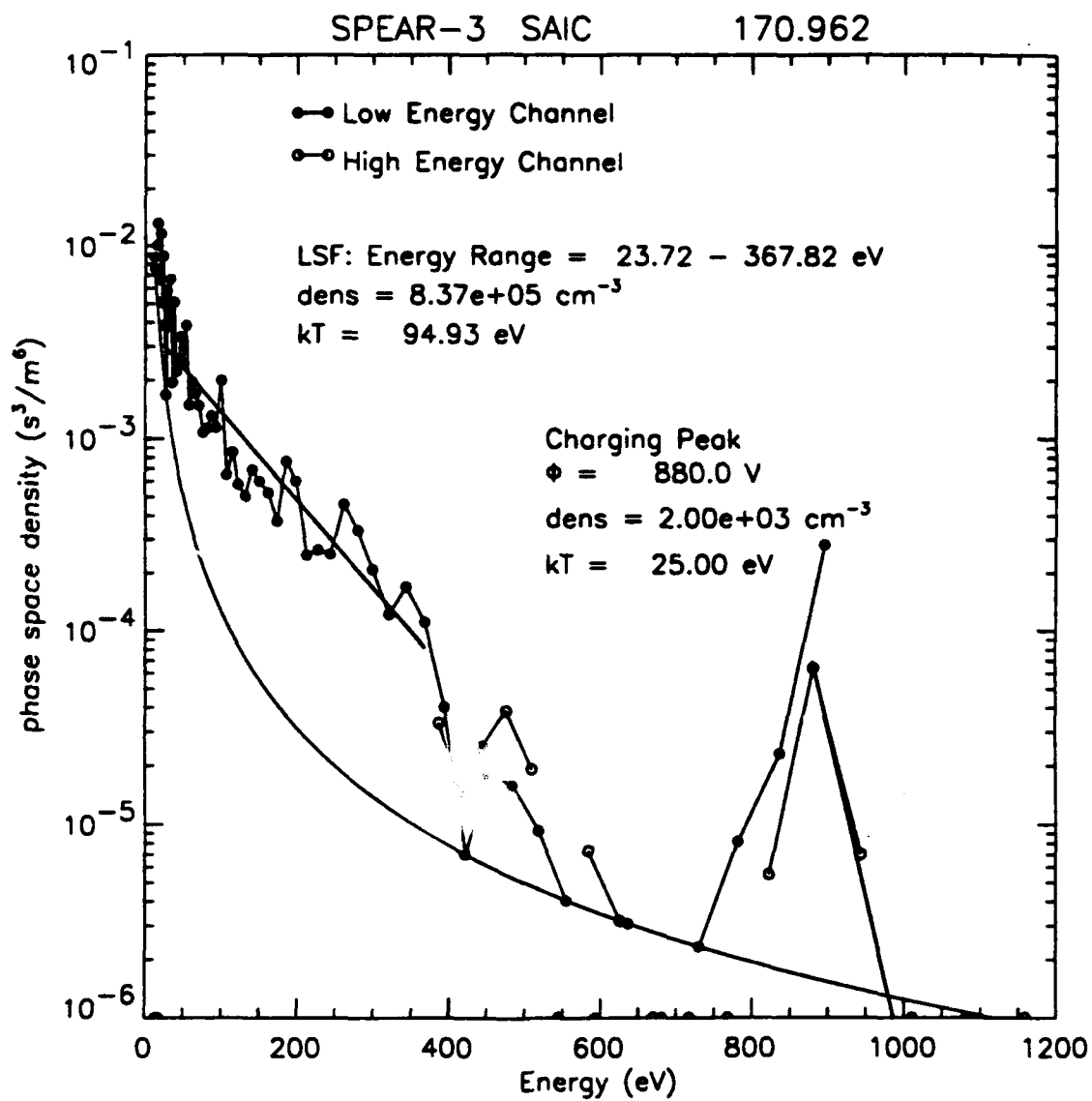


Figure 28. SPEAR III SAIC 170.962.

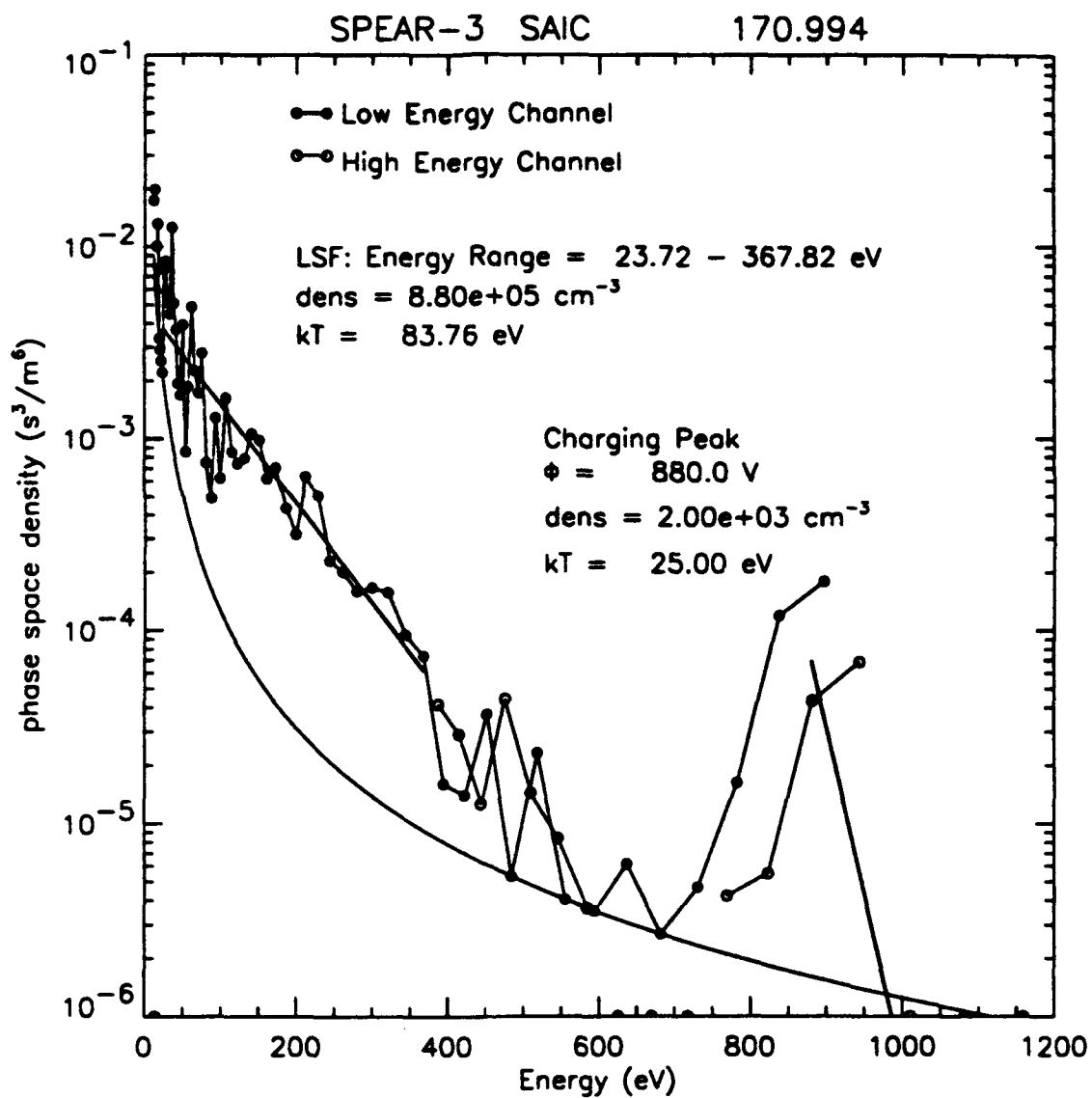


Figure 29. SPEAR III SAIC 170.994.

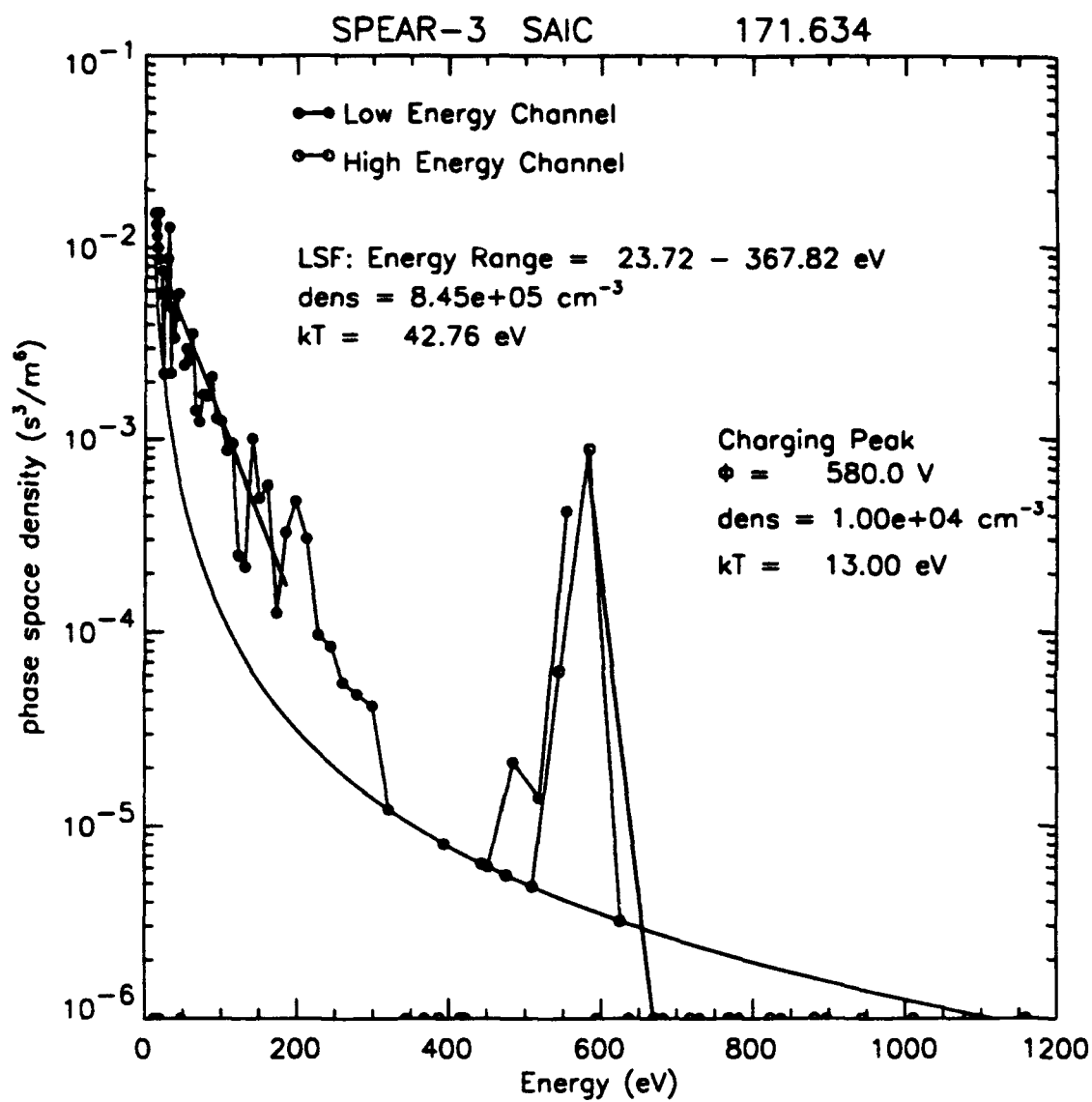


Figure 30. SPEAR III SAIC 171.634.

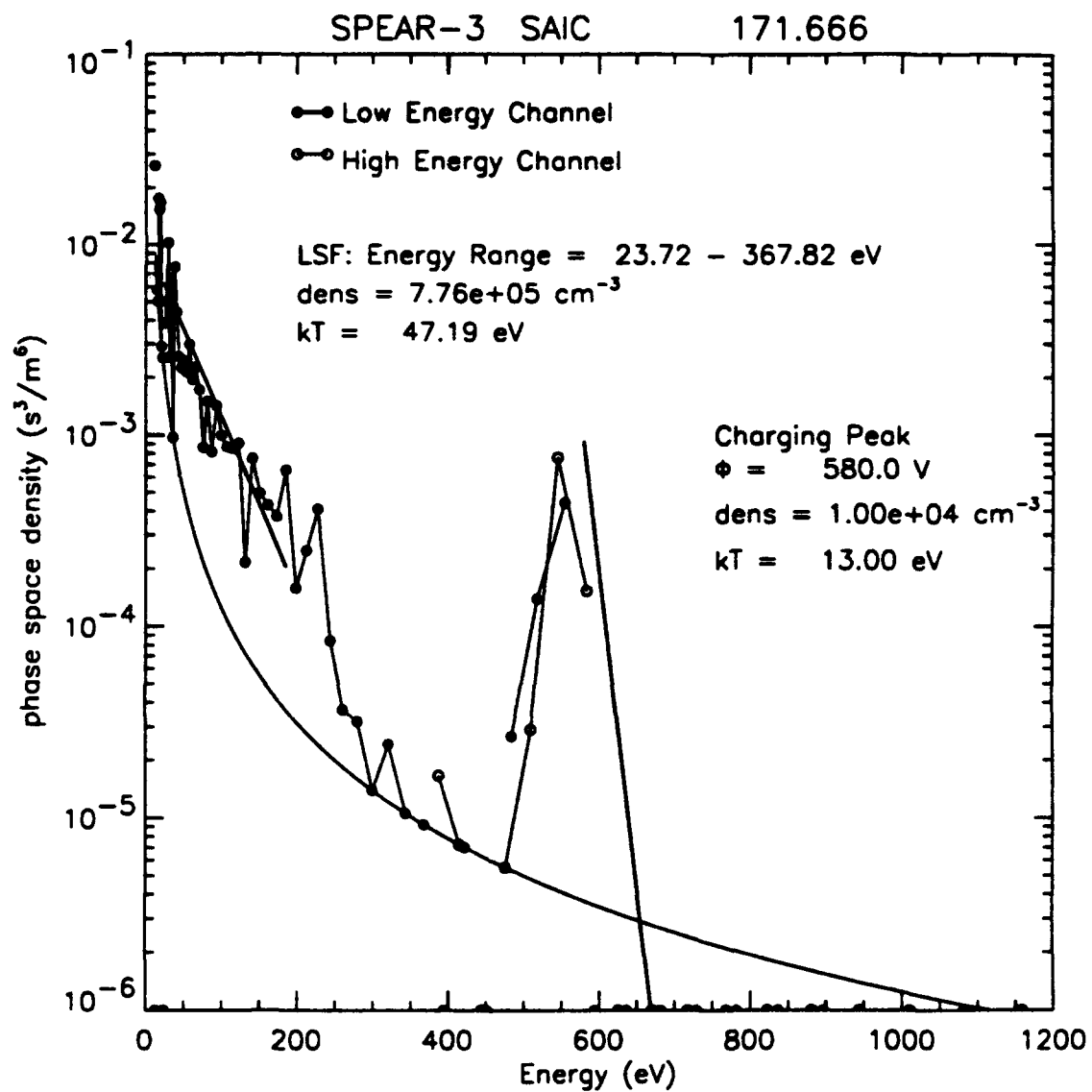
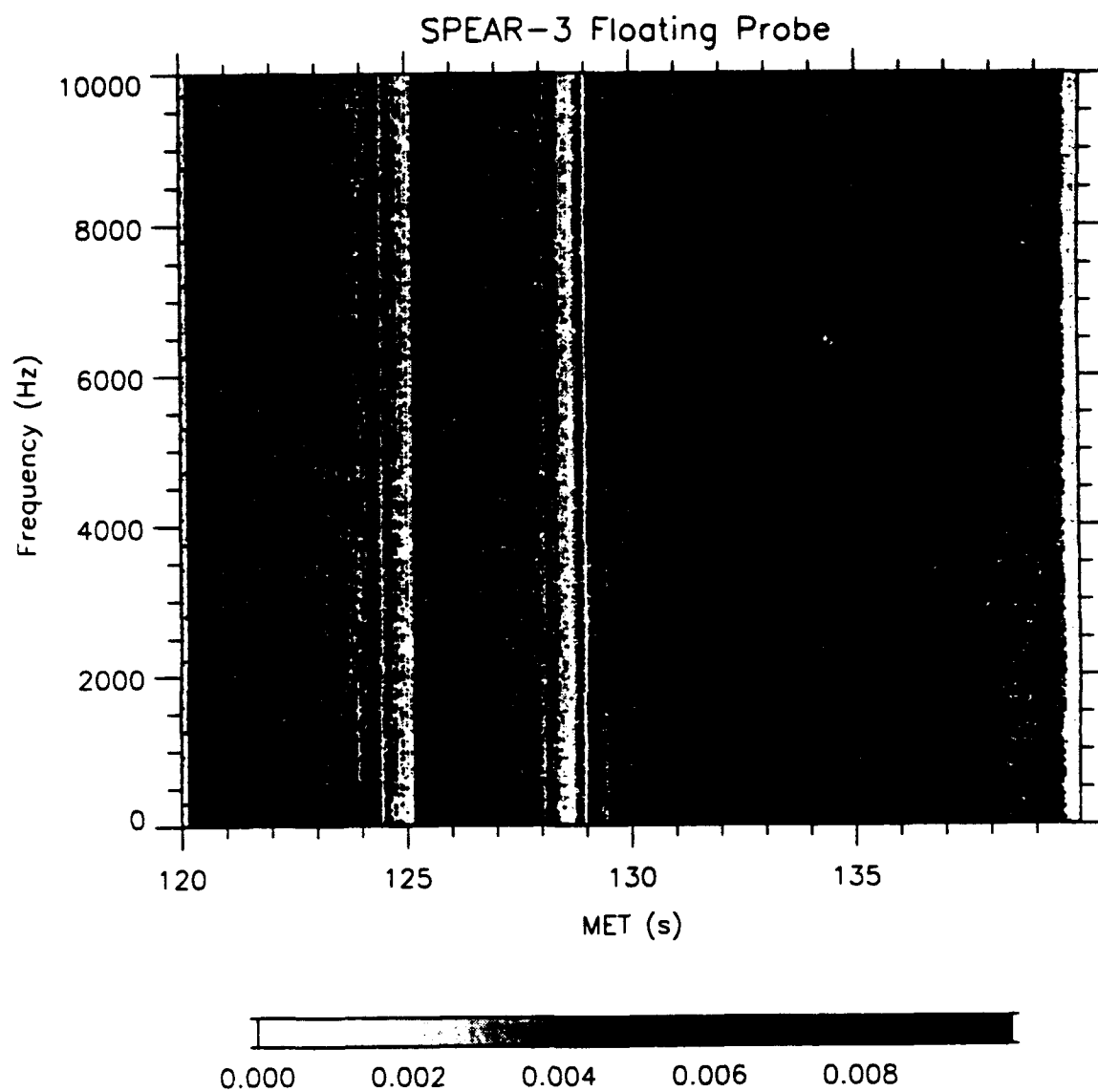


Figure 31. SPEAR III SAIC 171.666.



Naval Postgraduate School 14-Mar-1994 19:22:16.00

Figure 32. SPEAR III Floating Probe Spectrogram.

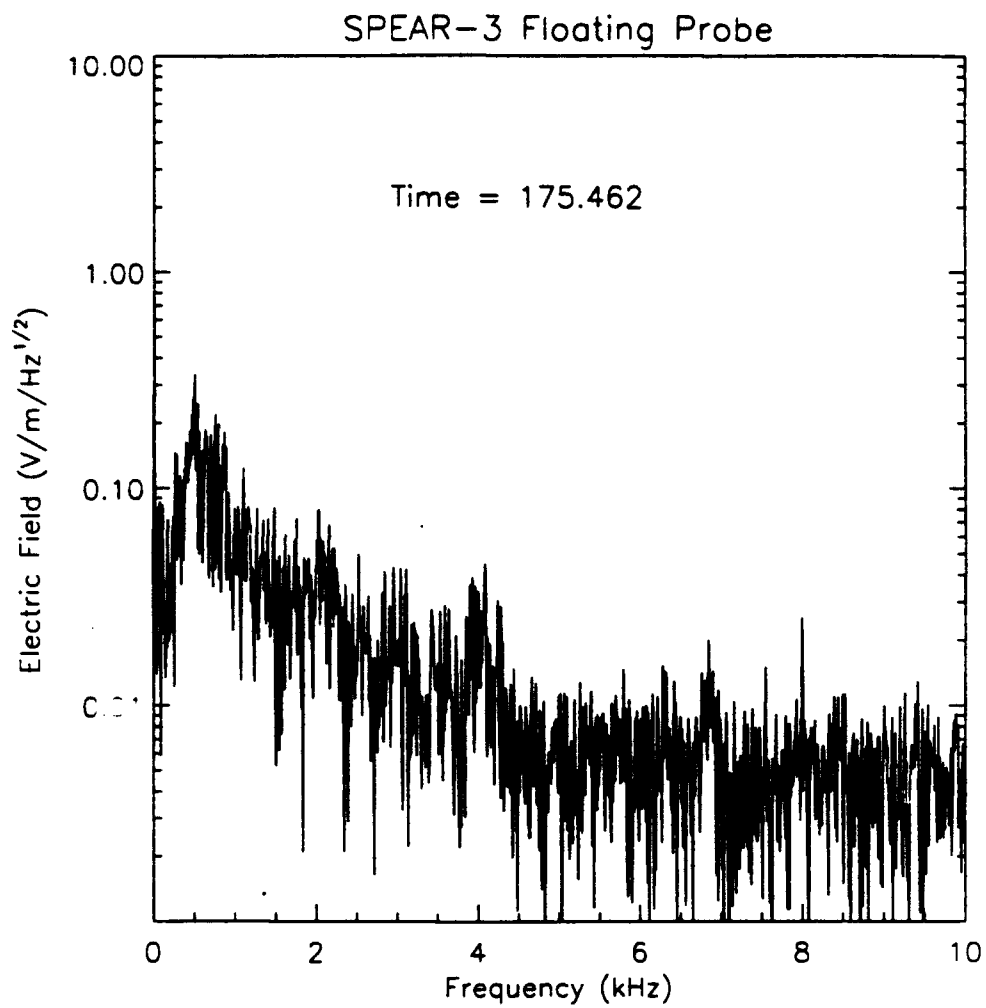
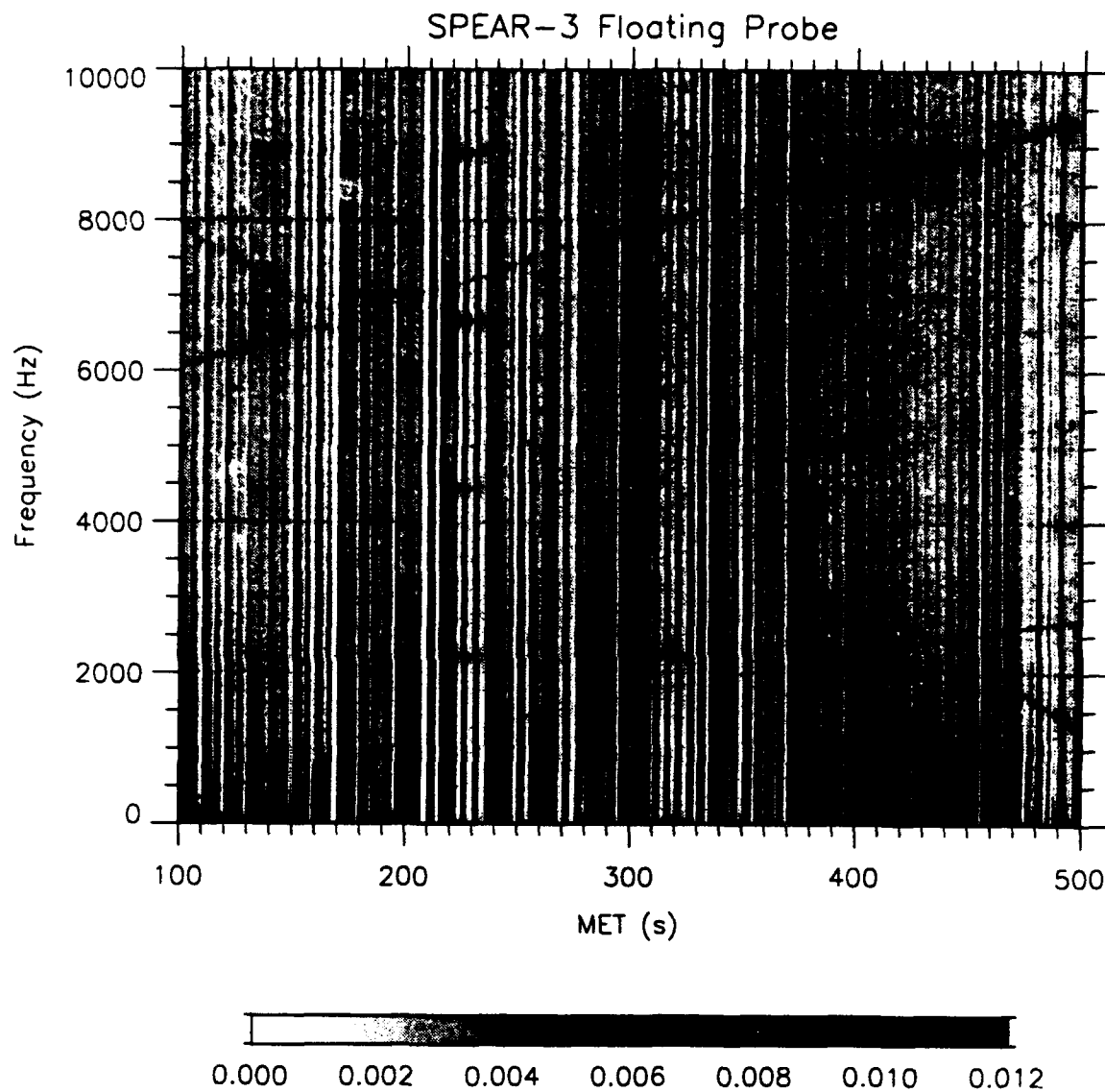
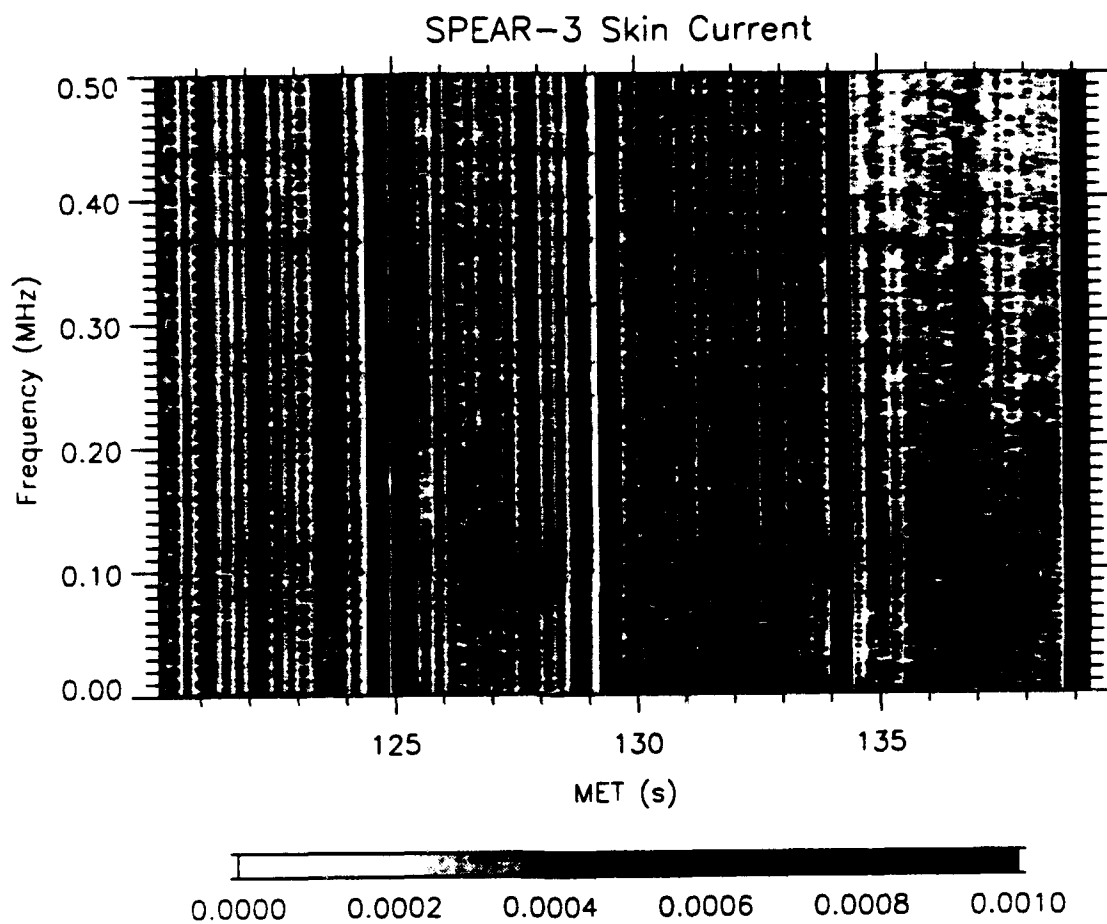


Figure 33. SPEAR III Floating Probe Line Plot.



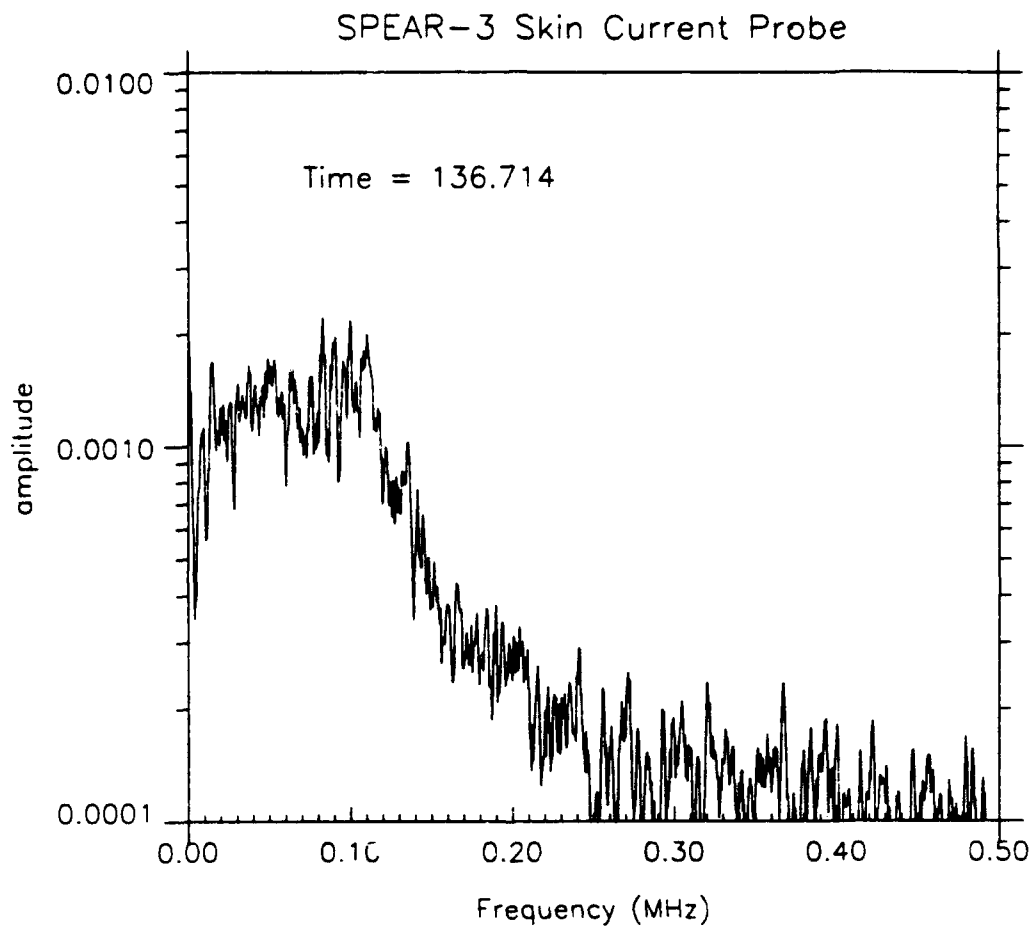
Naval Postgraduate School 23-Mar-1994 17:47:07.00

Figure 34. SPEAR III Floating Probe Spectrogram of Entire Flight.



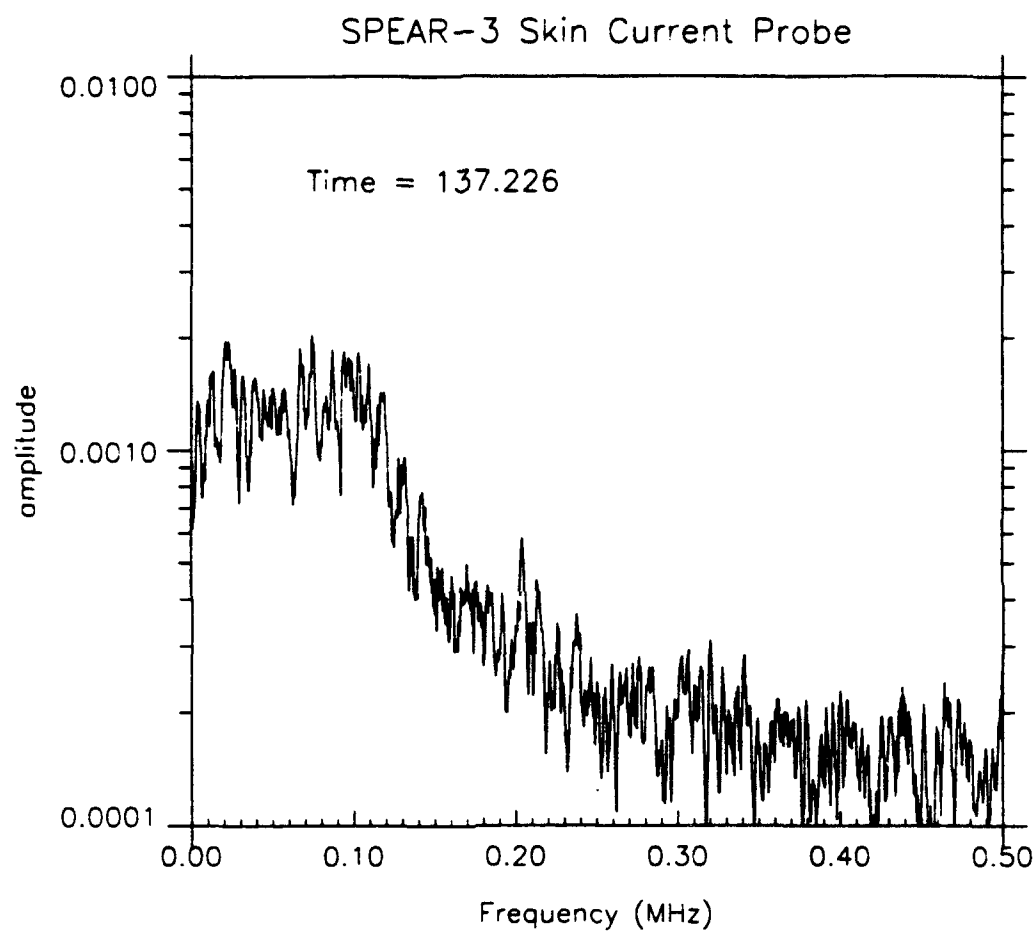
Naval Postgraduate School 14-Mar-1994 17:17:05.00

Figure 35. SPEAR III Skin Current Spectrogram.



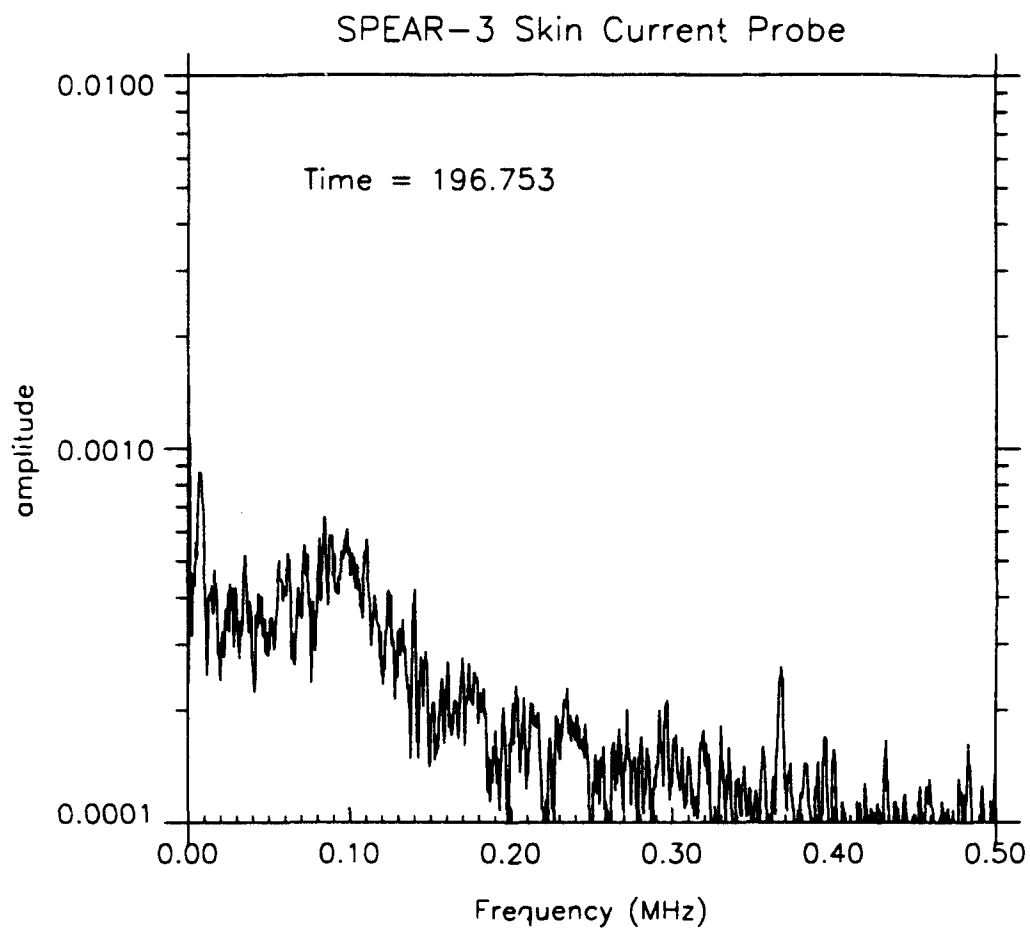
Naval Postgraduate School 14-Mar-1994 17:41:49.00

Figure 36. SPEAR III Skin Current Probe @ 134.714.



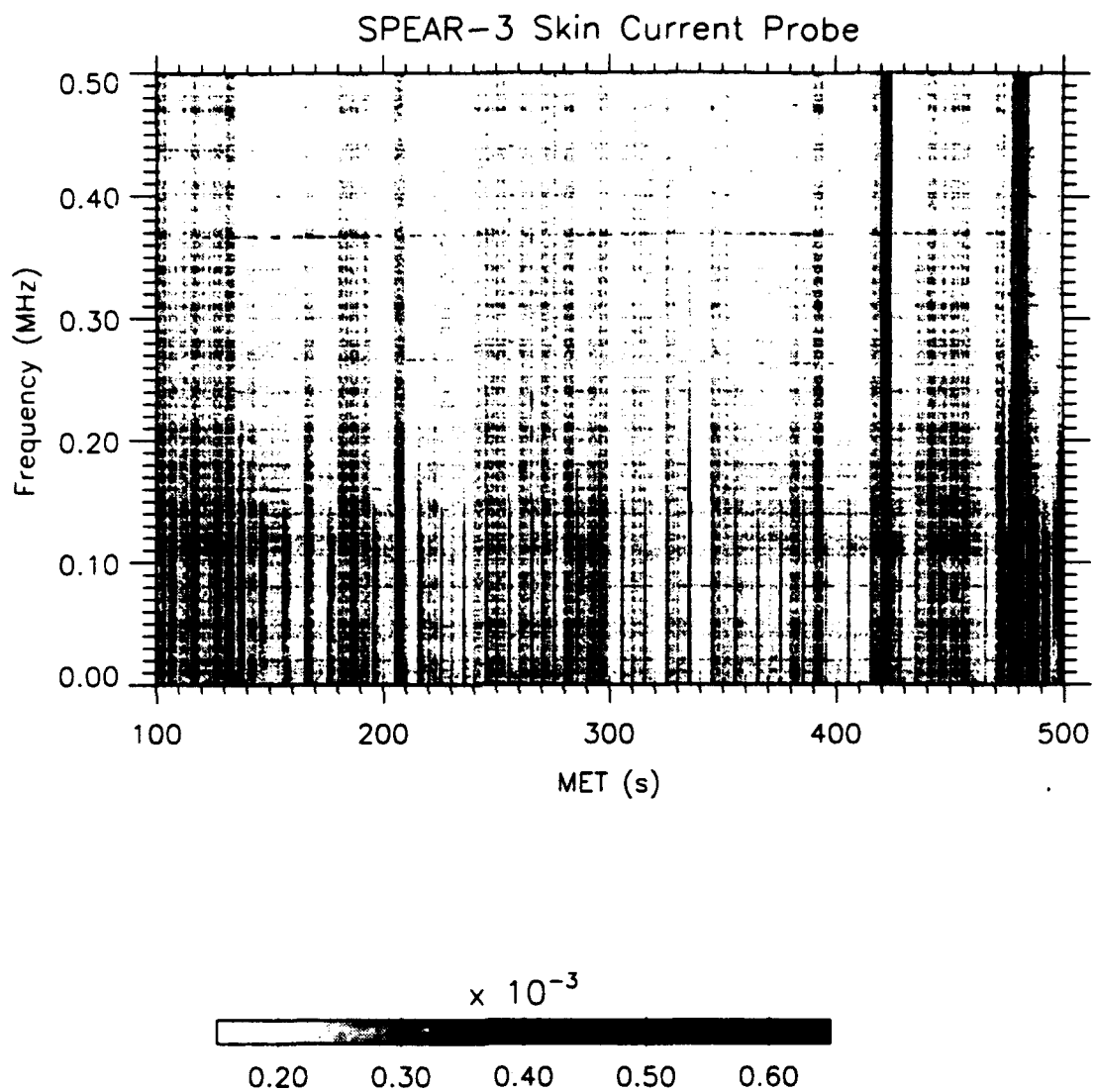
Naval Postgraduate School 14-Mar-1994 17:41:51.00

Figure 37. SPEAR III Skin Current Probe @ 137.226.



Naval Postgraduate School 14-Mar-1994 18:53:54.00

Figure 38. SPEAR III Skin Current Probe @ 196.753.



Naval Postgraduate School 23-Mar-1994 19:08:33.00

Figure 39. SPEAR III Skin Current Probe Spectrogram of Entire Flight.

LIST OF REFERENCES

¹Pake, George E., "Science and technology of directed energy weapons," Chairman Review Committee. Washington D.C.: American Physical Society, 1987. pp. 21-22.

²Ibid.

³Pake, pp. 23-34.

⁴Ibid.

⁵Neubert, T., Mandell, M. J., Sasaki, S., Gilchrist, B. E., Banks, P. M., Williamson, P. R., Raitt, W. J., Meyers, N. B., Oyama, K. I., & Katz, I., "the sheath structure around a negatively charged rocket payload," Journal of Geophysical Research. 95(A5), May 1, 1990. pp. 6156-6158.

⁶Pake, pp. 23-34.

⁷Allred, D. B., et. al., "The SPEAR I experiment high-voltage effects on space charging in the ionosphere," IEEE Transactions on Nuclear Science. 35(6). December 6, 1988. p. 1386.

⁸Neubert, pp. 6157-6164.

⁹Allred, p. 1386.

¹⁰SPEAR III Preliminary Design Review Data Package. Logan, Utah: Utah State University. June 3, 1991.

¹¹SPEAR III Preliminary Design Review Data Package. Logan, Utah: Utah State University, June 3, 1991.

¹²SPEAR III Preliminary ..., pp. 4-5.

¹³Ibid.

¹⁴Ibid.

¹⁵Ibid.

¹⁶Ibid.

¹⁷Ibid.

¹⁸From a conversation between the author and Douglas W. Potter, May 12, 1994.

¹⁹Ibid.

²⁰Ibid.

²¹Ibid.

²²Ibid.

²³Ibid.

²⁴SPEAR III Post Flight Data Review Meeting. Logan, Utah: Utah State University.

INITIAL DISTRIBUTION LIST

		<u>No. Copies</u>
1.	Defense Technical Information Center Cameron Station Alexandria, VA. 22304-6145	2
2.	Library, Code 52 Naval Postgraduate School Monterey, CA. 93943-5002	2
3.	Department Chairman, Code Ph Department of Physics Naval Postgraduate School Monterey, CA. 93943-5002	2
4.	Dr. R. C. Olsen, Code Ph/Os Department of Physics Naval Postgraduate School Monterey, CA. 93943-5002	5
5.	Dr. S. Gnanalingam, Code Ph/Gm Department of Physics Naval Postgraduate School Monterey, CA. 93943-5002	1
6.	Dr. I. Katz S-Cubed P. O. Box 1620 La Jolla, CA. 92038-1620	1
7.	Dr. M. Mandell S-Cubed P. O. Box 1620 La Jolla, CA. 92038-1620	1
8.	Space Systems Academic Group, Code 72 Naval Postgraduate School Monterey, CA. 93943-5002	1

9. **Space Systems Curricular Office, Code 61**
 Naval Postgraduate School
 Monterey, CA. 93943-5002
1
10. **Major Chuck Beatty**
 HQ/DNA/RAEV
 6801 Telegraph Road
 Alexandria, VA. 22310
1
11. **Dr. John Raitt**
 CASS
 Utah State University
 Logan, UT. 84322
2
12. **Dr. John Antoniadis**
 Naval Research Laboratory, Plasma Division
 Washington D. C. 20332
1
13. **Dr. Peter Palmadesso**
 Naval Research Laboratory, Plasma Division
 Washington D. C. 20332
1
14. **Dr. Paul Rodriguez**
 Naval Research Laboratory, Plasma Division
 Washington D. C. 20332
1
15. **Dr. Carl Sieftring**
 Naval Research Laboratory, Plasma Division
 Washington D. C. 20332
1
16. **Dr. Dave Walker**
 Naval Research Laboratory, Plasma Division
 Washington D. C. 20332
1
17. **Dr. Hugh R. Anderson**
 SAIC
 13400B Northrup Way, Suite 36
 Bellvue, WA. 98005
1
18. **Dr. Douglas W. Potter**
 SAIC
 13400B Northrup Way, Suite 36
 Bellvue, WA. 98005
1

19. **James H. Morris**
Department Head Class 133
Surface Warfare Officers School Command
446 Cushing Road
Newport, RI. 02841-1209

2